Time-frequency analysis of atrial fibrillation

Sandberg, Frida

2007

[Link to publication](#)

Time-Frequency Analysis of Atrial Fibrillation

Thesis for the degree of
Licentiate in Engineering

Frida Sandberg

Lund 2007

LUND INSTITUTE OF TECHNOLOGY
Lund University

Abstract

This licentiate thesis, containing two papers, is in the field of biomedical signal processing with main focus on signal processing of the ECG in patients with atrial fibrillation (AF). The two papers deal with different aspects of characterization of the f waves during atrial fibrillation. In the fist paper several measures designed to extract features of the f waves are evaluated with respect to their ability to predict spontaneous termination of paroxysmal AF. The fibrillation frequency, the variance of the fibrillation frequency, and the harmonic pattern of the f waves was found to differ significantly between terminating and non-terminating AF. In an independent test set, 90% of the signals were correctly classified using these measures. In the second paper, a method for improving robustness to noise when tracking the fibrillation frequency is presented. The method, which is based on an hidden Markov model (HMM), is evaluated using simulated AF mixed with different types of real noise obtained from ECG. The results show that the use of a HMM improves performance considerably by reducing the RMS error associated with frequency tracking: at 4 dB signal-to-noise ratio the RMS error drops from 0.2 Hz to 0.04 Hz.

Contents

Preface

This thesis consists of an introduction and two parts describing methods for predicting spontaneous termination of paroxysmal atrial fibrillation and robust frequency tracking of the fibrillation frequency. The two parts are based on the following two manuscripts:

1. F. Nilsson, M. Stridh, A. Bollmann, and L. Sörnmo, "Predicting spontaneous termination of atrial fibrillation using the surface ECG," *Med. Eng. Physics*, vol. 28, pp. 802–808, 2006.

2. F. Sandberg, M. Stridh, and L. Sörnmo, "Frequency tracking of Atrial Fibrillation using Hidden Markov Models," Submitted for publication.

Parts of the content have been published and presented at the following conferences:

3. F. Nilsson, M. Stridh, and L. Sörnmo, "Comparison of spectral properties in atrial signals using different QRST cancellation techniques," in *Proc. IFMBE*, Ischia, Italy, 2004.

4. F. Nilsson, M. Stridh, A. Bollmann, and L. Sörnmo, "Predicting spontaneous termination of atrial fibrillation using the surface ECG," in *Proc. Computers in Cardiology*, IEEE Press, pp. 657–660, Chicago, USA, 2004

5. F. Sandberg, M. Stridh, and L. Sörnmo, "Frequency tracking of Atrial Fibrillation using Hidden Markov Models," in *Proc. EMBS*, IEEE Press, pp. 1406–1409, New York, USA, 2006

Acknowledgments

First I would like to express my gratitude to my supervisor, Prof. Leif Sörnmo, for sharing his knowledge and experience with me, and for supporting and encouraging me during these years. He was the one that introduced me to the field of biomedical signal processing, and his catching enthusiasm was the reason I started my postgraduate studies.

I am also grateful to Dr. Martin Stridh, for all his help and support. His expertise on signal processing of atrial fibrillation gave me a head start on my work.

Thanks also to Ulrike Richter, Kristian Solem, Dr. Bengt Mandersson and the rest of the Signal Processing group for interesting discussions and valuable help. A special thanks to Ulrike, for making our room so nice and cosy.

I also wish to thank my other colleges and friends at the Dept. of Electroscience, specially to those in my corridor, for all the nice coffee breaks and lunches, which makes it fun to go to work in the morning.

Finally, I'm grateful to my friends and family for always supporting me. Thank you Peder for all love and support, you and Emil make me so happy.

Frida Sandberg

Introduction

1 Atrial Fibrillation

1.1 Anatomy of the Heart

The heart consists of a left and a right part, each incorporating two chambers; the atrium and the ventricle. The two sides are divided by a muscular wall, called the septum. Four different valves control the direction of the blood flow; the atrioventricular valves between the atria and the ventricles, and the pulmonary and aortic valves between the ventricles and the arteries. The wall of the heart, called myocardium, is mainly composed of muscle cells which exercise mechanical force during contraction. The mechanical force of the muscle cells is triggered by electrical impulses; a conduction system of specialized cells in the myocardium spreads the electrical impulse throughout the heart. Figure 1 shows the anatomy of the heart.
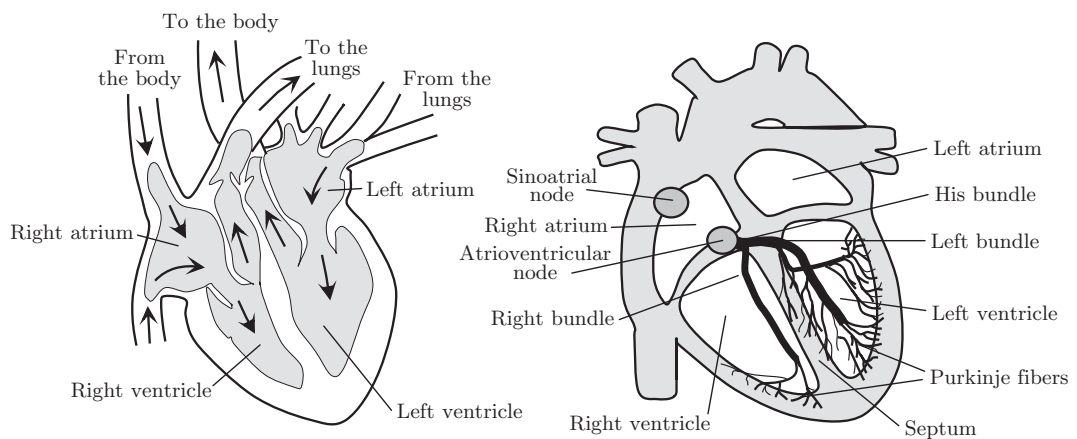
Figure 1: Anatomy of the heart [1].

During one cardiac cycle a sequence of mechanical events occur, starting when blood in the right atrium is forced into the right ventricle by contraction of the atria. The blood in the right atria has been collected from all veins in the body, except for the veins from the lungs. When the right ventricle is filled with blood, it contracts and forces the blood into the pulmonary artery, to the lungs where it is oxygenated. The oxygenated blood passes trough the pulmonary veins to the left atrium, which, once it is filled, contracts and forces the blood to the left ventricle. When the left ventricle contracts, the blood flows to all arterial vessels in the body, except for the lungs, into the venous system and back to the right atrium again.

The cardiac cycle consists of two phases; activation (contraction) and recovery (relaxation) which in electrical terms are referred to as depolarization and repolarization, respectively. Depolarization is a rapid change of the membrane potential of a cell, spreading to neighboring cells so that the electrical impulse propagates. After depolarization, the cell immediately starts its repolarization to return to its resting state. During this period of time, called refractory period, the cell cannot depolarize.

In the normal heart, the cardiac cycle is initiated by an electrical impulse originating from the sinoatrial (SA) node, the natural pacemaker of the heart situated in the right atrium. The electrical impulse propagates through the right and left atria to the atrioventricular (AV) node, where it is

collected and delayed before it continues to the bundle of His, being the only electrical connection between the AV node and the ventricles. The ventricular conduction system consists of the rapidly conducting left and right bundle branches and the Purkinje network. The rate of electrical impulses which causes the heart to beat is determined by the autonomic nervous system.

1.2   The Heart during Atrial Fibrillation

Atrial fibrillation (AF) is the most common sustained cardiac arrhythmia. It is labeled atrial tachy-arrhythmia, which means that the atria beats abnormally fast. The prevalence of AF increases with age, being less than 1% for people under 60 years of age, but more than 6% for those over 80 years [2]. AF may be sustained or paroxysmal, i.e., occasional episodes of fibrillation interrupt normal sinus rhythm. Sustained AF can be further divided into persistent AF, which may be terminated using certain treatment, and permanent AF.

In AF, the electrical impulse originates from different areas in the atria. This causes the atria to quiver rather than to contract, which results in insufficient heart function. The exact mechanisms of AF remains uncertain. The different theories involve two main processes: rapidly depolarizing foci, and reentry circuits. The rapidly depolarizing foci are usually located in the superior pulmonary veins, but can also occur in the right atria, or (more rarely) in superior vena cava or coronary sinus. The electrical impulses do not follow the normal conduction path, but instead they form electrical reentry loops in the atria. During AF, the refractory period of the conduction cells is usually shortened, and activation of the atrial conduction cells often occur immediately after the refractory period [3].

Of all electrical impulses coming from the atria during AF, only a limited number of signals actually reach the ventricles, since the AV node prevents the heart from racing. Still, the heart rate during AF is abnormally high. While AF is not generally considered life-threatening, there is a possibility of blood clots forming in the atria which leads to increased risk of stroke. One of every 6 strokes occur in patients with AF [2].

1.3   Diagnosis and Treatment

Atrial fibrillation is generally diagnosed from the surface ECG to confirm its presence. The medical history of the patient is also considered. In some patients transesophageal echocardiography is used in which ultrasound is employed to image heart anatomy and function. Invasive electrograms are normally only recorded if the patient is undergoing catheter ablation.

In recent onset episodes of AF, i.e., less than 48 hours, spontaneous termination is common. After 3 hours, 20% of the patients had converted to sinus rhythm, after 20 hours 60% had converted, and after 48 hours 80% had converted [4].

In paroxysmal AF, the treatment consists of suppression of paroxysms, heart rate control during AF, and long-term maintenance of sinus rhythm. Paroxysms may be suppressed using various drugs, e.g., flecanide and sotalol, which also help to maintain sinus rhythm. A serious side effect of these drugs is that they may induce other cardiac arrhythmias. The heart rate may be controlled using beta blockers [5].

Cardioversion denotes restoration of sinus rhythm in patients with persistent atrial fibrillation and can be achieved by means of electrical shock (electrical cardioversion) or drugs (pharmacological cardioversion). In more than 90% of recent onset AF, electrical cardioversion terminates AF. Electrical shocks are usually delivered noninvasively, but may also be delivered invasively. A wide range of drugs are used for pharmacological cardioversion, with varying efficacies. For recent onset AF, the success rate is about 50% 1.5 hour after drug administration. Pharmacological cardioversion is ineffective for AF longer than 7 days [4]. AF recurrence is common after cardioversion, and antiarrhythmic drugs are often needed for maintenance of sinus rhythm.

In permanent AF, the treatment consists of heart rate control and anticoagulants to prevent clots from forming in the atria. When using anticoagulation drugs, such as warfarin, dosage management is essential to obtain the right anticoagulation intensity. Computer programs for monitoring anti-coagulation can be used by the patient for self-testing and self-management of the anticoagulation therapy [6].

There are certain surgical procedures that may cure atrial fibrillation. In catheter ablation, energy is applied to burn the electrical paths so that the atria are segmented. Several different ablation techniques and a variety of energy sources may be used. One technique is to isolate the rapidly depolarizing foci. Since the foci are usually located in the pulmonary vein, isolation of this part is the most common focal ablation technique. Another idea is to obstruct the reentry path of the electrical impulses, thus forcing the electrical impulse into the correct path. The Maze operation is an open chest surgical procedure which segments the atria so that electrical reentry loops are no longer possible [7].

Atrial pacing has been used as a method of preventing and terminating atrial fibrillation [8, 9]. Implantable defibrillators provide the possibility for early and repeated cardioversion, which may prevent electrophysical remodeling of the heart [7]. A serious side effect of atrial pacing is that ventricular arrhythmia may be induced; this is one reason atrial pacing is no longer in use.

1.4   Challenges in Atrial Fibrillation

Today, there is no clinical test available that can predict the natural history of AF and the outcome of treatment. Since an ECG is recorded from practically all AF patients, it is desirable to classify AF from the ECG signal, to help physicians in deciding which treatment is appropriate for a specific patient. The characteristics of the ECG signal during AF varies not only between different patients, but also in the same patient over time. One important challenge is to track such changes in long term ECG recordings which usually are recorded during ambulatory conditions. Hence, the development of robust signal processing methods is essential.

2   Signal Processing in Atrial Fibrillation

2.1   ECG signal

The ECG is recorded by a number of electrodes attached to the body surface. The standard 12-lead ECG is acquired using ten electrodes, of which three are located on the wrists and ankle joints, and the remaining six are located on the chest. When recording the ECG continuously over longer periods of time, only three electrodes are often used.

During normal sinus rhythm, each heartbeat in the ECG signal consists of a P wave, a QRS complex and a T wave. The P wave corresponds to atrial activation, the QRS complex to activation of the ventricles, and the T wave to ventricular recovery, see Fig. 2 [10]. Two examples of ECG signals, recorded during normal sinus rhythm, are given in Figs. 3(a)–(b).

In atrial fibrillation, the P wave is replaced by an undulating baseline, where the waves are referred to as f waves. Two different examples of ECG signals during atrial fibrillation are given in Figs. 3(c)–(d). In atrial flutter, which is a closely related atrial tachyarrhythmia, the P waves are replaced by F waves which are slower and more regular than f waves during atrial fibrillation. An example of an ECG signal during atrial flutter is displayed in Fig. 3(e).
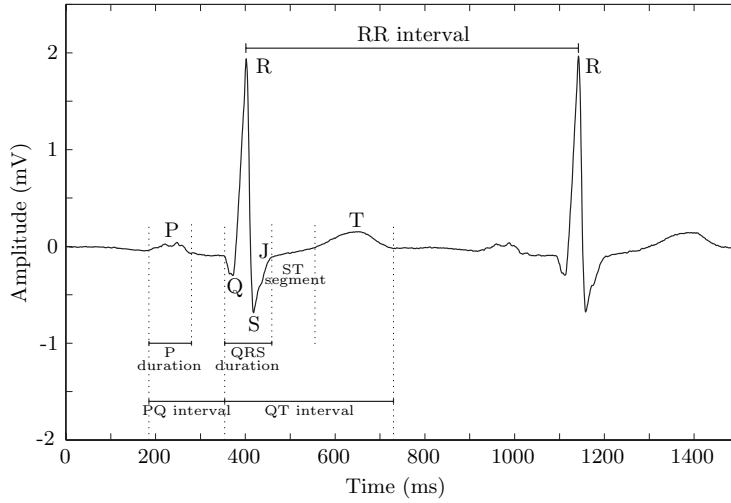
Figure 2: Different parts of the ECG signal during normal sinus rhythm.

2.2 Preprocessing

Baseline wander is a common artifact in the ECG signal, caused by varying electrode impedance during the recording due to, e.g., perspiration. Several techniques for removing this artifact has been presented, including time-invariant and time-varying linear filtering and polynomial fitting. Removing 50/60 Hz powerline interference, which is another common artifact in ECG signals, may be done using bandpass filtering since the spectral content of atrial activity typically is below 25 Hz. To obtain the ventricular rate, the QRS complexes need to be detected. This is usually done through a three-step process, consisting of linear filtering to suppress other parts of the ECG signal, a nonlinear transformation to enhance the QRS complex, and finally a decision rule to decide whether a QRS complex is present or not [1]. The QRS complexes are also classified according to their morphology, in order to determine which beats are ectopic.

2.3 RR intervals

The ventricular activity during AF can be studied through the RR intervals, i.e., the distance between two consecutive QRS complexes. The interval tachogram, defined as

$$d_{it}(k) = t_k - t_{k-1}, \quad k = 1, \dots, M, \tag{1}$$

where t_k defines the time of the k:th beat, contains the series of RR intervals. The variation of the RR intervals is commonly referred to as heart rate variability (HRV), and can be studied through a variety of measures.

During normal sinus rhythm, the ventricular rate is determined by the sinus node and, hence, by the autonomic nervous system. During AF, the ventricular rate does not only reflect autonomic modulation of the sinus node, but AV nodal refractoriness as well as the degree of concealed conduction. Therefore, the ventricular rate during AF is irregular, and the spectral content of the interval tachogram resembles that of white noise. Hence, HRV is almost always applied to evaluate autonomic modulation of the sinus rhythm before AF onset and after cardioversion [11].

A straightforward way to quantify HRV is to calculate the standard deviation of the RR intervals. An important consideration is then the number of intervals to include in the calculation, which determines if the measure reflects long term or short term HRV.
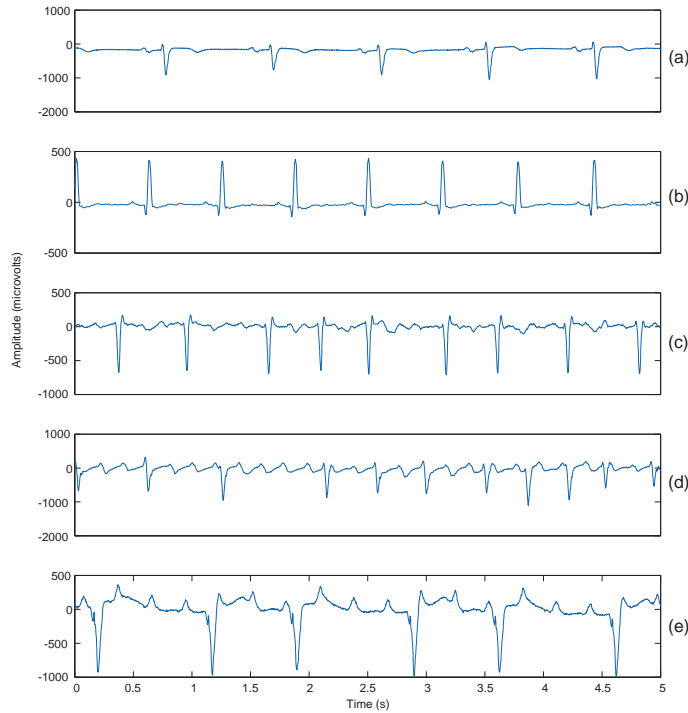
Figure 3: Different examples of ECG signals during (a)–(b) normal sinus rhythm, (c)–(d) atrial fibrillation, and (e) atrial flutter.

Spectral analysis is a popular approach to analyze HRV. Since the interval tachogram signal is indexed by interval number, k, power spectral analysis is not expressed in "cycles per second" (Hertz), but in "cycles per interval". If the interval function, $d_{if}(t_k)$, defined as the RR intervals function of their occurrence times, is instead used the spectral estimate can be expressed in Hertz. However, since the intervals are irregularly sampled, interpolation and resampling have to be done prior to applying the Fourier transform.

Autonomic modulation of the heart during normal sinus rhythm can be studied through HRV, since the low frequency content of HRV (0.04–0.15 Hz) is related to sympathetic activity, whereas the high frequency content (0.15–0.40 Hz) is mostly to parasympathetic activity. Transient alterations of the autonomic balance have been found to be associated with AF onset and recurrence.

Heart rate turbulence is a method that characterizes the short term oscillations in heart rate which follow atrial ectopic beats. Two measures, namely turbulence onset (TO) and turbulence slope (TS), are commonly used in heart rate turbulence analysis. Turbulence onset is the difference in mean RR interval prior to and after the ectopic beat, while TS is the maximum slope of the regression line in the series of RR intervals following the ectopic beat. Heart rate turbulence exhibits a different pattern prior to spontaneous AF onset which suggests that the turbulence is almost absent; TO was significantly larger and TS was significantly lower [12].

The autocovariance function, defined as

$$R_i = \frac{1}{(\bar{d}_{it})^2(N-i-1)} \sum_{j=0}^{N-i-1} (d_{it}(i+j) - \bar{d}_{it})(d_{it}(j) - \bar{d}_{it}), \tag{2}$$

where $\bar{d}_{it}$ is the mean length of the N intervals $d_{it}(k)$, measures the degree of correlation between subsequent RR intervals. During normal sinus rhythm, the covariance coefficients R_l are statistically significant, even at large l, while during AF the autocovariance function is only significant in R_1 compared to R_0 [13]. Hence, the RR intervals during AF are highly uncorrelated.

Analysis of RR interval histograms is limited to Holter recordings, since a large number of intervals is needed in order to construct a reliable histogram. The RR interval histogram during normal sinus rhythm is unimodal with a relatively narrow Gaussian shape, while the RR interval histogram during AF exhibits a variety of shapes [13]. In about 55% of the patients the RR interval histogram during AF shows two distinct peaks [14], where the two RR populations are believed to correspond to different electrical conduction routes.

Heart rate stratified histogram analysis (HRSH) is a technique with which histograms are stratified on the basis of the mean heart rate. The ECG signal is divided into segments that contain a fixed number of beats, for which the mean RR interval is calculated. RR intervals from segments with similar mean heart rate are then used to construct histograms [15]. Using HRSH, multiple RR distributions is more easily identified.

Lorenz plots have also been used when analyzing ventricular response during AF, i.e., individual RR intervals plotted against the corresponding preceding interval. Measures of the refractory period of the AV node [16], and concealed conduction [11] can be derived from such plots.

2.4   P Wave Analysis

The P waves can be analyzed during sinus rhythm between AF paroxysms or following cardioversion. In P wave analysis, the ECG signals are usually obtained from an orthogonal X, Y, Z lead system. Signal averaging is required to reduce the noise level, usually involving 200–350 beats. Following averaging, the different leads are combined into a vector magnitude from which the duration of the P wave, as well as the relative amplitude of different portions of the P wave, e.g., the last 10 ms, can be obtained. Signal averaged P wave analysis, as well as non-averaged P wave analysis, have been used in several studies to monitor and predict antiarrhythmic drug efficacy [17]. Prolonged P wave duration and late atrial potentials reflect disturbed atrial conduction, and are associated with higher AF recurrence [18] as well as transition from paroxysmal to chronic AF [19].

2.5   Atrial Activity Extraction

Atrial activity has much smaller magnitude than ventricular activity in the ECG signal. Hence, the ventricular activity needs to be cancelled before the atrial activity can be studied. Since the atrial and ventricular activities overlap spectrally, linear time-invariant filtering is unsuitable. Atrial activity extraction can be performed using various methods, including source separation methods [20, 21] and average beat subtraction methods [22, 23]. While the average beat subtraction methods extracts the atrial activity from a specific ECG lead, the source separation methods derive a global atrial signal with contributions from all leads. At least a 10-second long recording is needed to obtain a reliable average beat, while the source separation methods may be applied to shorter signals. The amplitude and frequency characteristics of the extracted atrial activity, using different extraction methods, were compared in [24].

Blind Source Separation Methods

When applying blind source separation methods to the ECG signal, each lead is assumed to consist of a linear combination of sources with atrial and ventricular origin and noise. The sources are considered independent since the atrial and the ventricular activities are decoupled during atrial fibrillation. Mathematically, the M observed ECG signals $\mathbf{x}(t) = [x_1(t), x_2(t), \ldots, x_M(t)]^T$ are given by

$$\mathbf{x}(t) = \mathbf{A}\mathbf{s}(t) \tag{3}$$

where $\mathbf{s}(t) = [s_1(t), s_2(t), \ldots, s_N(t)]^T$ are the N unknown independent sources, and $\mathbf{A}$ is an unknown mixing matrix. Hence, the sources can be estimated from the observed signals using

$$\hat{\mathbf{s}}(t) = \mathbf{W}\mathbf{x}(t). \tag{4}$$

Solving the blind source separation problem is therefore a matter of estimating the coefficients of the weight matrix $\mathbf{W}$. This is done by maximizing the independence between the estimated sources $\hat{\mathbf{s}} = [\hat{s}_1(t), \hat{s}_2(t), \ldots, \hat{s}_N(t)]^T$.

In independent component analysis (ICA), the independence of the sources are maximized based on higher order statistics or entropy measures. The sources are required to be non-Gaussian. Maximizing independence of the sources can be done by minimizing gaussianity of the sources, since sums of non-Gaussian variables are closer to Gaussian than the original signal according to the central limit theorem [25]. Gaussianity of a signal $\mathbf{y}$ can be measured using entropy, defined by

$$H(\mathbf{y}) = -\int p_{\mathbf{y}}(\boldsymbol{\eta}) \log p_{\mathbf{y}}(\boldsymbol{\eta}) d\boldsymbol{\eta}, \tag{5}$$

which is maximal if the vector has a Gaussian distribution. The signals are assumed to have zero mean, easily fixed by subtraction of the mean value, and to be white, i.e., uncorrelated with unit variance.

The fast ICA algorithm for estimating several independent components [25], using an iterative scheme to obtain the independent sources, has been employed to separate atrial activity from ventricular activity in the ECG signal [21]. Once the independent sources have been separated, each source needs to be identified as ventricular activity, atrial activity, or noise. The distribution of the different sources can be classified according to their gaussianity, which can be quantified using kurtosis,

$$\mathrm{kurt}(y) = E\{y^4\} - 3(E\{y^2\})^2. \tag{6}$$

Kurtosis is zero for Gaussian random variables, while sub-Gaussian variables, e.g., the uniform distribution, have negative kurtosis, and super-Gaussian variables, e.g., the Laplacian distribution, have positive kurtosis.

The sub-Gaussian sources are considered to be associated with atrial activity, while the super-Gaussian sources are ventricular activity, and the Gaussian sources are noise. Therefore the sources with the lowest kurtosis ($k < 0$) are considered to be atrial activity [21].

While ICA uses higher order statistics in solving the blind source separation problem, principal component analysis (PCA) uses only second order statistics, since the sources are assumed to be Gaussian.

In PCA the correlation between sources is minimized, being identical to maximizing the variance of the sources. Therefore, the first row of the mixing matrix $\mathbf{W}$, $\mathbf{w}_1$, should be chosen to maximize

$$E\{s_1^2(t)\} = E\{(\mathbf{w}_1^T \mathbf{x}(t))^2\} = \mathbf{w}_1^T E\{\mathbf{x}(t)\mathbf{x}(t)^T\}\mathbf{w}_1 = \mathbf{w}_1^T \mathbf{C}_x \mathbf{w}_1, \tag{7}$$

where the norm is constrained to be $||\mathbf{w}_1|| = 1$. The optimal solution to this is given by the first normalized eigenvector, $\mathbf{e}_1$, of the correlation matrix, $\mathbf{C}_x$. Hence, the first source $s_1(t)$ is given by

$\mathbf{e}_1^T \mathbf{x}(t)$. The following sources are chosen under the condition that they should be orthogonal to the previous sources, so that

$$E\{s_m(t)s_k(t)\} = E\{(\mathbf{w}_m^T \mathbf{x}(t))(\mathbf{w}_k^T \mathbf{x}(t))\} = \mathbf{w}_m^T \mathbf{C}_x \mathbf{w}_k = 0, \tag{8}$$

where $\mathbf{w}_m$ and $\mathbf{w}_k$ are m:th and k:th row of $\mathbf{W}$, respectively. The solution is given by the eigenvectors, so that $\mathbf{w}_k = \mathbf{e}_k$. Hence, using PCA, the rows of $\mathbf{W}$ are given by the eigenvectors of $\mathbf{C}_x$. Since PCA whitens the signal, it is often a preprocessing step in ICA algorithms.

Average Beat Subtraction Methods

Another approach for extracting atrial activity from ECG signals during AF is to subtract a template QRST complex from each QRST complex of the ECG signal. For this method to succeed, it is important that the QRST complex and the template are aligned in time and that they have similar morphology. The template QRST complex is obtained by averaging QRST complexes with similar morphologies. Spatiotemporal QRST cancellation is an extended form of average beat subtraction, where the beats are spatially aligned by shifting signal energy between the different leads. Spatiotempotal QRST cancellation has been shown to perform better than average beat subtraction with respect to the mean square error when applied to simulated AF [23], as well as the spectral properties of the extracted atrial activity using real ECG signals [26].

Each QRST complex is represented by a matrix $\mathbf{Y}_k$, which contains N samples from L leads. An average beat is calculated for every class of QRST-complexes. For each beat, $\mathbf{Y}_k$, the average beat, $\bar{\mathbf{X}}$, in the corresponding class is used to model the ventricular activity, $\hat{\mathbf{Y}}_k$, using

$$\hat{\mathbf{Y}}_k = \mathbf{J}_k \bar{\mathbf{X}} \mathbf{S}_k \tag{9}$$

where $\mathbf{J}_k$ is a time shift matrix and $\mathbf{S}_k$ is a spatial alignment matrix. The time shift matrix corrects for misalignment in time between the beat, $\mathbf{Y}_k$, and the averaged beat, $\bar{\mathbf{X}}$. The spatial alignment matrix is composed of a scaling matrix, $\mathbf{D}_k$, and a rotation matrix, $\mathbf{Q}_k$, i.e., $\mathbf{S}_k = \mathbf{D}_k \mathbf{Q}_k$. Therefore it can be used to compensate for shift variations in the electrical axis.

The atrial activity is assumed to be uncorrelated to the ventricular activity during atrial fibrillation. Hence, each beat can be modeled as a sum of ventricular activity, $\mathbf{Y}_V$, atrial activity, $\mathbf{Y}_A$, and noise, $\mathbf{W}$,

$$\mathbf{Y} = \mathbf{Y_V} + \mathbf{Y_A} + \mathbf{W}. \tag{10}$$

The aim is to estimate the parameters $\mathbf{Q}$, $\mathbf{D}$, and τ, so that

$$\mathbf{Y} - \mathbf{J}_\tau \bar{\mathbf{X}} \mathbf{S} = \mathbf{W}' + \mathbf{Y}_A. \tag{11}$$

Hence, the atrial activity and the noise will limit the performance of the QRST cancellation. To improve the cancellation performance, an estimate of the atrial activity $\tilde{\mathbf{Y}}_A$ is subtracted from the signal prior to QRST cancellation, so that

$$\mathbf{Z} = \mathbf{Y} - \tilde{\mathbf{Y}}_A \tag{12}$$

This procedure is referred to as AF reduction.

The cancellation parameters are estimated by solving the following minimization problem

$$\epsilon_{min}^2 = \min_{\mathbf{D}, \mathbf{Q}, \tau} ||\mathbf{Z} - \mathbf{J}_\tau \bar{\mathbf{X}} \mathbf{D} \mathbf{Q}||_F^2, \tag{13}$$

where $||\mathbf{A}||_F^2$ denotes the Frobenius norm, defined by $tr(\mathbf{A}\mathbf{A}^T)$. Since $\mathbf{Q}$ and $\mathbf{D}$ cannot be maximized independently, and a closed-form solution is difficult to find, the minimization problem is solved using an alternating, iterative approach.
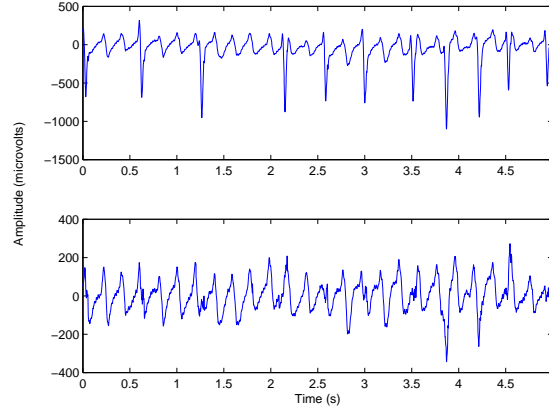
Figure 4: Example of ECG signal from a patient with AF (upper panel) and the corresponding QRST-cancelled residual ECG (lower panel). Note that the amplitude scale of the residual ECG is magnified.

The error can be expressed as

$$\epsilon^2 = tr(\mathbf{Z}\mathbf{Z}^T) + tr(\mathbf{J}_\tau \bar{\mathbf{X}}\mathbf{D}\mathbf{D}^T \bar{\mathbf{X}}^T \mathbf{J}_\tau) - 2tr(\mathbf{D}^T \bar{\mathbf{X}}^T \mathbf{J}_\tau \mathbf{Z}\mathbf{Q}^T). \tag{14}$$

Hence, minimization of ϵ^2 with respect to $\mathbf{Q}$, assuming that $\mathbf{D}$ is known, can be done by maximizing the last term. Singular value decomposition ($\mathbf{T} = \mathbf{U}\mathbf{\Sigma}\mathbf{V}$) of the matrix $\mathbf{T} = \mathbf{D}^T \bar{\mathbf{X}}^T \mathbf{J}_\tau \mathbf{Z}$, gives that the last term is maximized for

$$\hat{\mathbf{Q}} = \mathbf{U}\mathbf{V}^T. \tag{15}$$

Using the estimate of the rotation matrix, $\mathbf{Q}$, the error function can be rewritten

$$\epsilon_2 = tr(\mathbf{Z}'\mathbf{Z}') + tr(\mathbf{D}\mathbf{D}^T \bar{\mathbf{X}}^T \mathbf{J}_\tau^T \mathbf{J}_\tau \bar{\mathbf{X}}) - 2tr(\mathbf{D}^T \bar{\mathbf{X}}^T \mathbf{J}_\tau^T \mathbf{Z}') \tag{16}$$

where $\mathbf{Z}' = \mathbf{Z}\mathbf{Q}^{-1}$. Minimization of this expression with respect to $\mathbf{D}$ is done by setting the derivative to zero. Since $\mathbf{D}$ is a diagonal matrix, the derivatives of the diagonal elements should be set to zero,

$$\hat{d}_l = ([\mathbf{J}_\tau \bar{\mathbf{X}}]_l^T [\mathbf{J}_\tau \bar{\mathbf{X}}]_l)^{-1} ([\mathbf{J}_\tau \bar{\mathbf{X}}]_l^T [\mathbf{Z}']_l). \tag{17}$$

Using the estimate of $\mathbf{D}$, an improved estimate of $\mathbf{Q}$ can be obtained by minimizing (14). This alternating minimization procedure continues until the difference in error between two iterations is sufficiently small. The algorithm is initialized with $\mathbf{D_0} = \mathbf{I}$, i.e., no scaling, since it is desirable with a solution close to $\mathbf{Q} = \mathbf{D} = \mathbf{I}$. Minimization with respect to the time lag, τ, is done by a grid search in the interval $[-\Delta, \Delta]$; the smallest error when using optimal values of $\mathbf{Q}$ and $\mathbf{D}$ is chosen [23].

Finally, the optimally spatial and temporal aligned average beat is subtracted from each beat of the ECG, producing a residual signal like the one displayed in Fig. 4.

2.6 Atrial Fibrillation Feature Extraction

Several different features that characterizes the f waves may be extracted from the residual ECG signal. AF is often described as fine or coarse, referring to f wave amplitude. There is a large variability in f wave amplitude between different patients. However, no general differences have been found between the f wave amplitude in patients with permanent AF and with paroxysmal AF [27].

To quantify spatial organization, vector analysis has been applied to ECG signals during AF. Three-dimensional vector loops are constructed using ECGs from orthogonal leads, and each loop is characterized by its plane of best fit. The spatial organization is quantified based on the similarity of the planes [28].

3 Time-Frequency Analysis of Atrial Fibrillation

The rate of the fibrillation waves has been found to reflect the average refractory period of the atria [29]. The dominant fibrillation frequency can be obtained using the maximum peak of the power spectrum of the atrial signal [30]. The atrial refractory period, and hence the fibrillation frequency, is known to be affected by autonomic modulation. AF frequency has been used to monitor circadian variations as well as effects of parasympathetic and sympathetic stimulation. Studies show that the fibrillation frequency decrease during night and increase in the morning [31, 32], and that both carotide sinus massage (parasympathetic stimulation) [33] and head-up tilt (sympathetic stimulation) [34] altered the fibrillation frequency.

The fibrillation frequency can also be used to predict spontaneous AF behavior and therapeutic effects. Several studies have demonstrated significant correlation between AF frequency and the likelihood of spontaneous or drug-induced AF termination. A low fibrillation frequency has proved to be a good predictor of spontaneous AF termination [35]. When the fibrillation frequency is below 6 Hz the likelihood of successful pharmaceutical cardioversion is higher [36, 37]. The risk of early AF recurrence is also higher for patients with higher AF frequency [38]. These are important considerations when selecting candidates for cardioversion.

3.1 Short Time Fourier Transform

To explore the time-varying properties of AF, time-frequency analysis is needed. The basic approach to time-frequency analysis is to segment the signal and calculate the Fourier spectra for each segment (Welch's method). The short-time Fourier transform is defined by

$$W_{STFT}(n,k) = \sum_{m=-K/2+1}^{K/2} s(m-n)w(m)e^{-j2\pi km}, \tag{18}$$

where $s(n)$ is the signal, $w(n)$ is a window function, and K is the window length and the number of frequency samples. The segments may be overlapping. A larger value of K gives better frequency resolution, but poorer time resolution. Hence, the choice of segment size is a trade-off between time and frequency resolution.

3.2 Other Time-Frequency Distributions

While the STFT depends linearly on the signal, there are other time-frequency distributions that depend quadratically of the signal, e.g., the Wigner-Ville distribution (WVD), defined by

$$W_{WVD}(n,k) = \sum_{m=-L}^{L} \sum_{l=-L}^{L} A_z(m,l)e^{-j2\pi ln/N}e^{-j2\pi km/N}, \tag{19}$$

where the ambiguity function

$$A_z(m,l) = \sum_{p=-L}^{L} z(p+m)z^*(p-m)e^{j2\pi lp/N} \tag{20}$$

and $z(n)$ is the analytic equivalent of the signal $s(n)$,

$$z(n) = s(n) + j\mathcal{H}(s(n)) \tag{21}$$

where $\mathcal{H}(s(n))$ is the Hilbert transform of $s(n)$. The advantage of these quadratically dependent distributions is the improved time-frequency resolution. However, quadratic distributions of multicomponent signals introduce cross-terms.

There are other quadratic distributions, e.g., the Choi-Williams distribution (CWD), which are similar to the WVD except for that the different regions of the ambiguity plane are weighted down using a kernel function, $f(m,l)$, so that

$$W_{CWD}(n,k) = \sum_{m=-L}^{L} \sum_{l=-L}^{L} f(m,l) A_z(m,l) e^{-j2\pi ln/N} e^{-j2\pi km/N}. \tag{22}$$

In the CWD the kernel, defined by

$$f(m,l) = e^{-\frac{m^2 l^2}{\sigma}}, \tag{23}$$

weights down cross-terms between different frequency components.

3.3 Cross-Wigner-Ville Distribution

The Cross-Wigner-Ville distribution (XWVD) is defined by

$$W_{XWVD}(n,k) = \sum_{m=-L}^{L} \sum_{l=-L}^{L} A_{z_1,z_2}(m,l) e^{-j2\pi ln/N} e^{-j2\pi km/N}, \tag{24}$$

where

$$A_{z_1,z_2}(m,l) = \sum_{p=-L}^{L} z_1(p+m) z_2^*(p-m) e^{j2\pi lp/N} \tag{25}$$

and with $z_1(n)$ and $z_2(n)$ as analytical signals, may be used to extract the local frequency of a time-varying, repetitive signal.

Instantaneous frequency estimation can be performed using the XWVD with an iterative procedure. First, a preliminary frequency trend, $\hat{F}_0$, is determined using, e.g., the STFT or the WVD. Then:

1. A frequency-modulated sinusoid is reconstructed from the frequency trend.

$$z_{\hat{F}_l}(n) = e^{j2\pi \sum_{i=0}^{n} \hat{F}_l(i)} \tag{26}$$

2. The XWVD between $z_{\hat{F}_l}$ and $z(n)$ is computed by

$$W_{XWVD_{l+1}}(n,k) = \sum_{m=-L}^{L} \sum_{l=-L}^{L} z(p+m) z_{\hat{F}_l}^*(p-m) e^{-j4\pi mk/K} \tag{27}$$

   Peak detection in the XWVD domain results in a new frequency trend, $\hat{F}_{l+1}$.

3. The procedure is repeated until the frequency trend converges

$$\hat{F}_{l+1}(n) - \hat{F}_l(n) = 0 \forall n \tag{28}$$

The cross-term between the original signal and the reconstructed sinusoid is large, and hence selected when reconstructing a new sinusoid. In this way, the reconstructed sinusoid will converge to the frequency trend of the original signal [39]. A disadvantage of the XWVD approach is that only the fundamental frequency of AF is being used, while the harmonic pattern is not considered when characterizing the AF frequency.

3.4   Spectral Profile

The spectral profile method makes use of the harmonic pattern of AF to robustify AF frequency trend estimation [40]. The ECG signal is divided into overlapping segments, for which the spectrum, $\mathbf{q}_l$, is obtained using a nonuniform Fourier transform,

$$\mathbf{q}_l = \mathbf{FW}\mathbf{x}_l, \tag{29}$$

where the elements of the $N \times N$ diagonal matrix $\mathbf{W}$ defines a window function. The $K \times N$ matrix $\mathbf{F}$ defines the K-point discrete, nonuniform Fourier transform

$$\mathbf{F} \quad = \quad \begin{bmatrix} \mathbf{1} & e^{-j2\pi\mathbf{f}} & e^{-j2\pi\mathbf{f}2} & \cdots & e^{-j2\pi\mathbf{f}(N-1)} \end{bmatrix}, \tag{30}$$

where $\mathbf{f} = [f_0 \cdots f_{K-1}]^T$ is a logarithmically scaled frequency vector, given by

$$f_k = f_0 \cdot 10^{\frac{k}{K}}, \quad k = 0, \dots, K-1. \tag{31}$$

Each observed spectrum $\mathbf{q}_l$ can be modeled by $\tilde{\mathbf{q}}_l$ being a frequency-shifted, θ_l, and amplitude-scaled, a_l, version of a known real-valued spectral profile, $\boldsymbol{\phi}_l$,

$$\tilde{\mathbf{q}}_l = a_l \mathbf{J}_{\theta_l} \boldsymbol{\phi}_l, \tag{32}$$

where the matrix $\mathbf{J}_{\theta_l}$ performs the frequency shift by selecting the appropriate interval of $\boldsymbol{\phi}_l$. The amplitude parameter a_l and the frequency-shift parameter θ_l can be estimated by minimizing the quadratic cost function, $J(\theta_l, a_l)$, so that the model, $\tilde{\mathbf{q}}_l$, optimally matches the true spectrum, $\mathbf{q}_l$,

$$J(\theta_l, a_l) \quad = \quad (\mathbf{q}_l - \tilde{\mathbf{q}}_l)^T \mathbf{D} (\mathbf{q}_l - \tilde{\mathbf{q}}_l) \tag{33}$$

$$= \quad (\mathbf{q}_l - a_l \mathbf{J}_{\theta_l} \boldsymbol{\phi}_l)^T \mathbf{D} (\mathbf{q}_l - a_l \mathbf{J}_{\theta_l} \boldsymbol{\phi}_l), \tag{34}$$

where $\mathbf{D}$ is a $K \times K$ diagonal matrix designed to weight the error of the frequency components differently, in order to compensate for the logarithmic frequency scaling. Minimization of (8) results in an estimator of the frequency-shift,

$$\hat{\theta}_l = \arg\max_{\theta_l} \left[\mathbf{q}_l^T \mathbf{D}^{\frac{1}{2}} \mathbf{J}_{\theta_l} \mathbf{D}^{\frac{1}{2}} \boldsymbol{\phi}_l \right]. \tag{35}$$

Using the peak position of the spectral profile and the frequency-shift estimate, a robust frequency estimate is obtained.

An estimator of the amplitude can also be obtained by minimizing the cost function (8),

$$\hat{a}_l = \mathbf{q}_l^T \mathbf{D}^{\frac{1}{2}} \mathbf{J}_{\hat{\theta}_l} \mathbf{D}^{\frac{1}{2}} \boldsymbol{\phi}_l. \tag{36}$$

With the estimates of a_l and θ_l, a model of the spectrum is obtained,

$$\hat{\mathbf{q}}_l = \hat{a}_l \mathbf{J}_{\hat{\theta}_l} \boldsymbol{\phi}_l. \tag{37}$$

The spectral profile is gradually updated to fit the shape of the true spectrum. For the first segment, the spectral profile, $\boldsymbol{\phi}_0$, is initiated by

$$\boldsymbol{\phi}_0 \quad = \quad \begin{bmatrix} 0.01 & \cdots & 0.01 & 1 & 0.01 & \cdots & 0.01 \end{bmatrix}^T, \tag{38}$$

where $\boldsymbol{\phi}_0$ is 1 at the peak position and 0.01 at all other positions. The spectral profile, $\boldsymbol{\phi}_l$, is then updated for each segment through exponential averaging so that

$$\hat{\boldsymbol{\phi}}_{l+1} = (1 - \alpha_l)\hat{\boldsymbol{\phi}}_l + \alpha_l \frac{\mathbf{J}_{\hat{\theta}_l} \hat{\mathbf{q}}_l}{\|\mathbf{J}_{\hat{\theta}_l} \hat{\mathbf{q}}_l\|}, \quad l > 0, \tag{39}$$

where the gain α_l $(0 < \alpha_l < 1)$ is set to a positive value when the signal is judged reliable, and otherwise zero. To determine if the l:th segment is reliable, i.e., contains AF, measures based on $\mathbf{q}_l$ and $\hat{\mathbf{q}}_l$ are employed. A segment is accepted as AF if 1) the SNR is sufficiently large, 2) the model error exhibits no sudden increase, 3) the second largest peak has neither too high a magnitude, nor 4) is too close to the position of the fundamental frequency.

Other measures that characterizes the spectral content of the atrial activity, such as the exponential decay of the harmonics, γ_l, may be extracted from the spectral profile. Although the spectral profile method is more robust to noise than the previously described methods, it may fail in estimating the AF frequency in noisy ECG signals, e.g., recorded during ambulatory conditions.

4 Hidden Markov Model

A Hidden Markov model (HMM) for frequency tracking may be used as a postprocessing step to robustify frequency tracking of AF in noisy signals. A Markov model consists of a finite number of states, with predefined state transition probabilities. The likelihood of a certain state, corresponding to a unique set of observed variables, depends only on the previous state (random walk). In an HMM the state variables cannot be directly observed. Each state is associated with certain observation probabilities, i.e., the probabilities of observing a specific set of variables. Given the sequence of observations of an HMM, the optimal state sequence can be obtained using the Viterbi algorithm or the Forward-Backward algorithm.

4.1 Frequency Tracking using HMM

Given an observed sequence of frequency estimates, $\mathbf{z} = [z(1), z(2), \ldots, z(T)]^T$, the goal is to obtain the true sequence, denoted $\mathbf{x} = [x(1), x(2), \ldots, x(T)]^T$. The HMM for frequency tracking includes one zero state, $z(t) = 0$, when no signal is present, and $P - 1$ different frequency states, $z(t) = 1, \ldots, P - 1$, where state i includes frequencies between f_i and $f_i + \Delta f = f_{i+1}$, with a center frequency of $\tilde{f}_i$,

$$\tilde{f}_i = f_i + \frac{\Delta f}{2}. \tag{40}$$

An HMM is completely characterized by its state transition matrix $\mathbf{A}$, its observation matrix $\mathbf{B}$, and its initial state vector $\mathbf{\Pi}$ [41]. The state transition matrix $\mathbf{A}$ describes a priori knowledge of transition probabilities between different states. When designing an HMM for AF frequency tracking, it is assumed that the AF frequency changes by a Gaussian distribution, so that it is more likely that the AF frequency remains the same or changes gradually than abruptly. Hence, the transition probability between non-zero states is given by

$$a_{ij} = \frac{(1 - v)g_{ij}}{\sum_{k=1}^{P} g_{ik}}, \quad i, j = 1, 2, \ldots, P - 1, \tag{41}$$

where

$$g_{ij} = \frac{1}{d\sqrt{2\pi}} \int_{f_j}^{f_j + \Delta f} \exp\left[-\frac{(f - \bar{f}_i)^2}{2d^2}\right] df. \tag{42}$$

The width of the Gaussian distribution, d, is a design parameter determined by the likelihood of AF frequency change.

Furthermore, it is assumed that the probability of AF being present in the signal is high, so that the initiation probability, u, is high and the termination probability, v, is low. The probabilities of

initiation and termination are assumed to be equal for all frequencies, so that

$$a_{00} = 1 - u \tag{43}$$

$$a_{0j} = \frac{u}{P-1}, \quad j = 1, 2, \ldots, P-1 \tag{44}$$

$$a_{j0} = v, \quad j = 1, 2, \ldots, P-1 \tag{45}$$

The observation matrix, $\mathbf{B}$, describes the probabilities of observing a specific frequency given the true AF frequency. Assuming the signal is a sinusoid with added white noise, these probabilities can be determined using a priori knowledge of the frequency estimation method, the detection threshold, D, and the SNR, defined by the signal amplitude, a, and the noise variance, σ^2. If no AF is present, the probabilities of no detection and inaccurate detection in state i are given by

$$b_{00} = \prod_{i=1}^{P-1} \int_0^D p_2(r) dr = \left[1 - e^{-\frac{D^2 N}{\sigma^2}} \right]^{P-1}, \tag{46}$$

$$b_{0i} = \frac{1 - b_{00}}{P-1}, \tag{47}$$

respectively. If a fibrillation frequency between f_m and f_{m+1} is present, the probabilities of correct detection, no detection, and inaccurate detection are given by

$$b_{mm} = \int_D^\infty p_1(r) \prod_{i=1, i \neq m}^{P-1} \int_0^r p_2(r_1) dr_1 dr = \int_D^\infty p_1(r) \cdot \left[1 - e^{-\frac{r^2 N}{\sigma^2}} \right]^{P-2} dr, \tag{48}$$

$$b_{m0} = \int_0^D p_1(r) dr \prod_{i=1, i \neq m}^{P-1} \int_0^D p_2(r) dr = \left[1 - e^{-\frac{D^2 N}{\sigma^2}} \right]^{P-2} \int_0^D p_1(r) dr, \tag{49}$$

$$b_{m, i \neq m} = \frac{1 - b_{m0} - b_{mm}}{P-2}, \tag{50}$$

respectively. The functions $p_1(r)$ and $p_2(r)$ are probability density functions (PDFs) of the magnitude of the STFT at frequency f. If a signal with frequency f is present, the PDF is given by

$$p_1(R(f)) = \frac{2R(f)N}{\sigma^2} \cdot I_0 \left(\frac{R(f)aN}{\sigma^2} \right) \cdot e^{-\frac{N(4R(f)^2 + a^2)}{4\sigma^2}}, \tag{51}$$

and if not the PDF is given by

$$p_2(R(f)) = \frac{2R(f)N}{\sigma^2} \cdot e^{-\frac{NR(f)^2}{\sigma^2}}. \tag{52}$$

The initial state vector is set to $\mathbf{\Pi} = [a_{00}, a_{01}, \ldots, a_{0n}]$, i.e., start in zero state, to force automatic track initiation.

Based on the state transition matrix, $\mathbf{A}$, the observation matrix, $\mathbf{B}$, and the initial state vector, $\mathbf{\Pi}$, the Viterbi algorithm determines an optimal state sequence, $\mathbf{x}$, given the observed sequence, $\mathbf{z}$. This algorithm is initialized for $0 \leq j \leq P-1$ with

$$\delta_1(j) = \ln \pi_j + \ln b_{j, z(1)}, \tag{53}$$

$$\psi_1(j) = 0, \tag{54}$$

where $\boldsymbol{\pi}$ is the initial state vector, $b_{j, z(1)}$ is element $(j, z(1))$ of $\mathbf{B}$, and $z(1)$ is the first element of the observed sequence, $\mathbf{z}$. Then, for $t = 2, 3, \ldots, T$

$$\delta_t(j) = \ln b_{j, z(t)} + \max_{0 \leq i \leq P-1} \left(\delta_{t-1}(i) + \ln a_{ij} \right), \tag{55}$$

$$\psi_t(j) = \arg \max_{0 \leq i \leq P-1} \left(\delta_{t-1}(i) + \ln a_{ij} \right), \tag{56}$$

are defined for $0 \leq j \leq P - 1$, where $b_{j,z(t)}$ is element $(j, z(t))$ of $\mathbf{B}$, $z(t)$ is element number t of the observed sequence, and a_{ij} is element (i, j) of $\mathbf{A}$. The optimal sequence, $\mathbf{x}$ is obtained using

$$x(T) = \arg \max_{0 \leq j \leq P-1} (\delta_T(j)), \tag{57}$$

$$x(t) = \psi_{t+1}(x(t+1)). \tag{58}$$

Frequency estimates that differs from the frequency trend are excluded or replaced by the HMM, resulting in a more robust frequency estimation method. Robust frequency tracking is of interest in many other fields, e.g., radar and sonar. HMM-based frequency tracking of an isolated sinusoidal tone embedded in white noise was originally presented in [42].

5   Summary of Included Papers

5.1   Predicting Spontaneous Termination of Atrial Fibrillation using the Surface ECG

Extracting features that characterize AF from the surface ECG is important when trying to help physicians diagnosing the arrhythmia. The purpose of this work was to extract features from AF that could predict spontaneous termination. Time-varying measures, such as amplitude, wave morphology, and frequency, as well as complexity measures were investigated.

A database of 80 one-minute segments extracted from 20–24 hour two-channel Holter ECG recordings was used in the study. The signals were classified as either non-terminating (N), soon-terminating (S), or immediately terminating (T). The database was divided into a training set of 30 recordings (10N, 10S and 10T), and two test sets of 30 recordings (N and T) and 20 recordings (S and T), respectively.

Preprocessing of the signals consisted of baseline and 50 Hz filtering. The atrial activity of the ECG signal was extracted using spatiotemporal QRST cancellation.
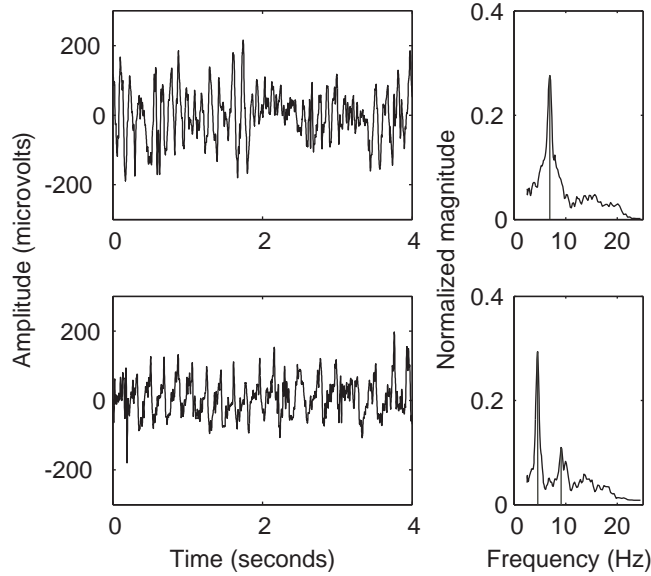
Using the log-spectral profile method, the fibrillation frequency, f_l, fibrillation amplitude, a_l, and exponential decay, γ_l, was obtained for each segment l of 128 samples (2.56 seconds). A validity measure was employed to check if the segments contained atrial activity. Following exclusion of occasional episodes of sinus rhythm and local noise using the validity measure, the measurements of the remaining segments were averaged to produce reliable estimates of the fibrillatory frequency, $\bar{f}$, the exponential decay, $\bar{\gamma}$, and the peak amplitude, $\bar{a}$. Variation of the fibrillatory frequency, σ_f, is described by the standard deviation of the fibrillatory frequency. If more than 75% of the signal segments were invalid, the entire recording was excluded from further analysis.

Three different complexity measures were also examined; spectral entropy, $\mathcal{H}_{SpE}$, sample entropy, $\mathcal{H}_{SaE}$, and fractional spectral radius, $\mathcal{H}_{FSR}$. The spectral entropy, $\mathcal{H}_{SpE}$, quantifies the spectral complexity of a signal, $x(n)$, and is obtained by applying Shannon's entropy to the probability density function of the signal. A large value of $\mathcal{H}_{SpE}$ indicates high complexity of $x(n)$. The sample entropy, $\mathcal{H}_{SaE}$, compares similarity in fixed length segments of the signal. A large value of $\mathcal{H}_{SaE}$ indicates high complexity of $x(n)$. The fractional spectral radius, $\mathcal{H}_{FSR}$, is another complexity measure which gives an upper bound to the trajectory dimension. A small value of $\mathcal{H}_{FSR}$ indicates a large trajectory dimension, and hence high complexity of $x(n)$.

The measurements were compared for the different groups of the training set. We found that the fibrillation frequency, the variance of the fibrillation frequency, and the exponential decay significantly differed between the non-terminating (N) and the terminating (T) AF patients, as shown in Tab. 1. Neither the fibrillation amplitude nor the complexity measures differed between the groups. Figure 5 shows examples of residual ECGs of non-terminating and terminating AF and their corresponding spectral profile, from which the significant measures are derived.

Table 1: Mean value and standard deviation of measurements used for AF characterization, for the non-terminating (N) and immediately-terminating (T) signals in the training set. Measures with boldface asymptotic p-values are significantly different according to a Kolmogorov-Smirnov test.

Measurement average	N $Mean \pm Std$	T $Mean \pm Std$	Asymptotic p-value
$\bar{f}$	6.91 ± 0.66	5.00 ± 0.65	**0.000033**
$\bar{\gamma}$	1.29 ± 0.27	0.79 ± 0.20	**0.0021**
σ_f	0.80 ± 0.23	0.52 ± 0.13	**0.0127**
$\bar{a}$	21.7 ± 12.4	28.6 ± 16.7	N.S.
$\mathcal{H}_{SpE}$	1.73 ± 0.34	1.73 ± 0.18	N.S.
$\mathcal{H}_{SaE}$	1.51 ± 0.34	1.63 ± 0.16	N.S.
$\mathcal{H}_{FSR}$	0.16 ± 0.04	0.14 ± 0.02	N.S.

Figure 5: Residual ECGs (left) with different exponential decay, $\bar{\gamma}$, fibrillatory frequency, $\bar{f}$, and variation of fibrillatory frequency, σ_f and corresponding spectral profile, ϕ_l (right). (a) Non-terminating AF with $\bar{\gamma} = 1.6$, $\bar{f} = 7.6$ Hz and $\sigma_f = 0.9$, and (b) terminating AF with $\bar{\gamma} = 0.7$, $\bar{f} = 5.0$ Hz, $\sigma_f = 0.4$.

Table 2: Mean value and standard deviation of measurements used for AF characterization, from the soon-terminating (S) and immediately-terminating (T) signals in the training set.

Measurement average	S $Mean \pm Std$	T $Mean \pm Std$	Asymptotic p-value
$\bar{f}$	5.33 ± 0.65	5.00 ± 0.65	N.S.
$\bar{\gamma}$	0.90 ± 0.17	0.79 ± 0.20	N.S.
σ_f	0.67 ± 0.32	0.52 ± 0.13	N.S.
$\bar{a}$	32.3 ± 17.8	28.6 ± 16.7	N.S.
$SpecEn$	1.74 ± 0.16	1.73 ± 0.18	N.S.
$SampEn$	1.61 ± 0.12	1.63 ± 0.16	N.S.
FSR	0.16 ± 0.03	0.14 ± 0.02	N.S.

There were no significant differences between any of the measures obtained from the soon-terminating (S) and the immediately-terminating (T) signals of the training set, as shown in Table 2.

The three significant measures were highly correlated. Hence, only the most significant measure, $\bar{f}$, was used to predict spontaneous termination. Using this predictor, 90% of the test set was correctly classified into N and T.

5.2 Frequency Tracking of Atrial Fibrillation using Hidden Markov Models

Inaccurate AF frequency estimates is a problem, especially in ambulatory ECG recordings, where the signal is often corrupted with noise. The purpose of this study was to make AF frequency trend estimation more robust to noise by post-processing the frequency estimates using an HMM which make use of a priori knowledge. The state transition matrix incorporates a priori knowledge of AF characteristics, such as the rate of AF frequency change, while the observation matrix incorporates a priori knowledge of the frequency estimation, e.g., SNR and detection threshold.

Simulated AF mixed with noise to different SNR was used in the evaluation. White noise as well as real noise obtained from ECG recordings were used. The frequency estimates were calculated using the STFT. An example of frequency tracking using HMM of simulated AF, mixed with noise obtained from a real ECG recording to different SNR, is displayed in Fig. 12. At 10 dB SNR all frequencies were correctly estimated by the STFT, thus using the HMM has no effect. At 5 dB SNR two inaccurate frequency estimates were excluded and two inaccurate frequency estimates were replaced by the HMM. At 0 dB SNR several inaccurate estimates were either excluded or replaced by the HMM.

An average RMS error of the frequency estimates was obtained using simulated AF with different frequency trends. The average RMS error of the estimated frequencies of simulated AF signals, mixed with noise obtained from real ECG recordings, is presented in Fig. 15. A high zero state occupancy percentage tend to give a lower average RMS error, since the error is undefined at zero state. Therefore, it is important to compare not only the average RMS error, but also the zero state occupancy percentage. The RMS error of the frequency estimates using HMM is compared to that of the spectral profile method, showing that the HMM performs better at low SNR.
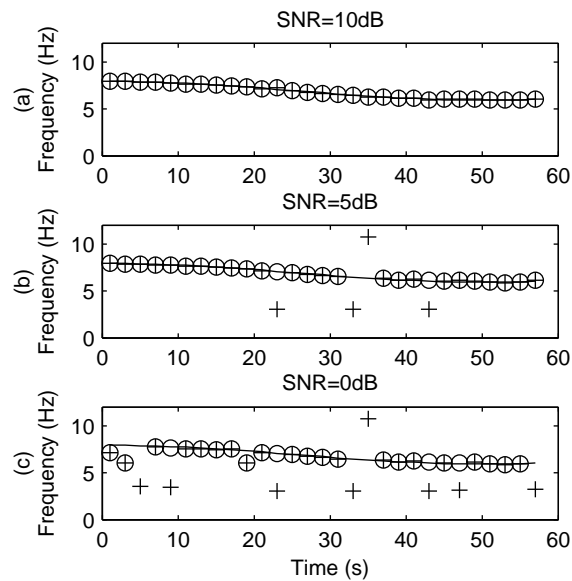
Figure 6: Frequency tracking with and without employing the HMM of simulated AF signals mixed with QRST-noise to (a) 10 dB SNR, (b) 5 dB SNR and (c) 0 dB SNR. Solid line shows the actual frequency trend, '+' the estimated frequency of the mixed signal, and 'o' the estimated frequency of the mixed signal using HMM. Absent '+' or 'o' corresponds to zero state.
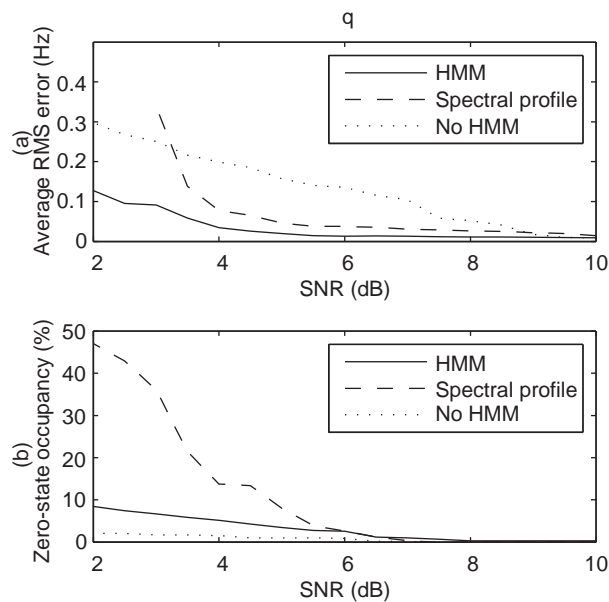
Figure 7: (a) RMS error and (b) zero state occupancy as function of SNR for simulated AF with QRST remainders.

References

[1] L. Sörnmo and P. Laguna, *Bioelectrical signal processing in cardiac and neurological applications*. Elsevier, 2005.

[2] V. Fuster *et al.*, "ACC/AHA/ESC guidelines for the management of patients with atrial fibrillation," *Circ.*, vol. 104, pp. 2118–2150, 2001.

[3] S. Nattel, "New ideas about atrial fibrillation 50 years on," *Nature*, vol. 415, pp. 219–226, 2002.

[4] S. Nattel and L. Opie, "Controversies in cardiology 3: Controversies in atrial fibrillation," *Lancet*, vol. 367, pp. 262–72, 2006.

[5] G. Lip and S. Kamath, "Atrial fibrillation (2): Antiarrhythmic agents," *The Pharmaceutical Journal*, vol. 264, pp. 659–663, 2000.

[6] ——, "Atrial fibrillation (3): Antithrombotic therapy," *The Pharmaceutical Journal*, vol. 264, pp. 773–777, 2000.

[7] D. Zipes and J. Jalife, *Cardiac Electrophysiology: From Cell To Bedside*. W B Saunders company, 2004.

[8] C. Israel, G. Grönefeldt, Y. Li, and S. Hohnloser, "Usefulness of atrial pacing for prevention and termination of atrial thcyarrhythmias in a patient with atrial fibrillation," *PACE*, vol. 25, pp. 1527–1529, 2002.

[9] C. Schmitt, G. Ndrepepa, S. Weyerbrock, C. Kolb, and B. Zrenner, "Pseudotermination of intermittent atrial fibrillation by a pacemaker algorithm," *PACE*, vol. 24, pp. 1824–1826, 2001.

[10] G. Wagner, *Practical Electrocardiography*, 9th ed. Williams & Wilkins, 1994.

[11] A. Bollmann *et al.*, "Analysis of surface electrocardiograms in atrial fibrillation: techniques, research, and clinical applications," *Europace*, vol. 8, pp. 911–926, 2006.

[12] S. Vikman *et al.*, "Heart rate turbulence after atrial premature beats before spontaneous onset of atrial fibrillation," *J. Am. Coll. Cardiol.*, vol. 45, pp. 278–284, 2005.

[13] R. J. Cohen, R. D. Berger, and T. Dushane, "A quantitative model for the ventricular response during atrial fibrillation," *IEEE Trans. Biomed. Eng.*, vol. 30, pp. 769–781, 1983.

[14] S. Rokas *et al.*, "Atrioventricular node modification in patients with chronic atrial fibrillation: role of morphology of rr interval variation," *Circ.*, vol. 103, pp. 2942–2948, 2001.

[15] N. Cai, M. Dohnal, and S. B. Olsson, "Methodological aspects of the use of heart rate stratified RR interval histograms in the analysis of atrioventricular conduction during atrial fibrillation," *Cardiovasc. Res.*, vol. 21, pp. 455–462, 1987.

[16] J. Billette, R. Nadeau, and F. Roberge, "Relation between the minimum RR interval during atrial fibrillation and the functional refrectory period of the AV junction," *Cardiovasc. Res.*, vol. 8, pp. 347–351, 1974.

[17] I. Kubara, H. Ikeda, T. Hiraki, T. Yoshida, M. Ohga, and T. Imaizumi, "Dispersion of filtered p wave duration by p wave signal-averaged ECG mapping system: Its usefulness for determining efficacy of disopyramide on paroxysmal atrial fibrillation," *J. Cardiovasc. Electrophysiol.*, vol. 10, pp. 670–679, 1999.

[18] M. Raitt, K. Ingram, and S. M. Thurman, "Signal-averaged p wave duration predicts early recurrence of atrial fibrillation after cardioversion," *Pacing Clin. Electrophysiol.*, vol. 23, pp. 259–265, 2000.

[19] Y. Abe *et al.*, "Prediction of transition to chronic atrial fibrillation in patients with paroxysmal atrial fibrillation by signal averaged electrocardiography: A prospective study," *Circ.*, vol. 96, pp. 2612–2616, 1997.

[20] P. Langley, J. P. Bourke, and A. Murray, "Frequency analysis of atrial fibrillation," in *Proc. Computers in Cardiology*. IEEE Press, 2000, pp. 65–68.

[21] J. J. Rieta, V. Zarzoso, J. Millet-Roig, R. Garcia-Civera, and R. Ruiz-Granell, "Atrial activity extraction based on blind source separation as an alternative QRST cancellation for atrial fibrillation analysis," in *Proc. Computers in Cardiology*. IEEE Press, 2000, pp. 69–72.

[22] J. Slocum, E. Byrom, L. McCarthy, A. Sahakian, and S. Swiryn, "Computer detection of atrioventricular dissociation from surface electrocardiograms during wide QRS complex tachycardia," *Circ.*, vol. 72, pp. 1028–1036, 1985.

[23] M. Stridh and L. Sörnmo, "Spatiotemporal QRST cancellation techniques for analysis of atrial fibrillation," *IEEE Trans. Biomed. Eng.*, vol. 48, pp. 105–111, 2001.

[24] P. Langley, J. J. Rieta, M. Stridh, J. Millet, L. Sörnmo, and A. Murray, "Comparison of atrial signal extraction algorithms in 12-lead ECGs with atrial fibrillation," *IEEE Trans. Biomed. Eng.*, vol. 53, pp. 343–346, 2006.

[25] A. Hyvarinen, J. Karhunen, and E. Oja, *Independent Component Analysis*. Wiley Interscience, 2001.

[26] F. Nilsson, M. Stridh, and L. Sörnmo, "Comparison of spectral properties in atrial signals using different QRST cancellation techniques," in *Proc. IFMBE*, vol. 6, 2004.

[27] Q. Xi, A. Sahakian, T. Frohlich, J. Ng, and S. Swiryn, "Relationship between patterns of occurence of atrial fibrillation and surface electrocardiographic fibrillatory wave characteristics," *Heart rhythm*, vol. 1, pp. 656–663, 2004.

[28] J. Ng, A. Sahakian, W. Fisher, and S. Swiryn, "Surface ECG vector characteristics of organized and disorganized atrial activity during atrial fibrillation," *J. Electrocardiol.*, vol. 37, pp. 91–97, 2004.

[29] A. Capucci, M. Biffi, and G. Boriani, "Dynamic electrophysiological behaviour of human atria during paroxysmal atrial fibrillation," *Circ.*, vol. 92, pp. 1193–1202, 1995.

[30] M. Holm, S. Pehrsson, M. Ingemansson, L. Sörnmo, R. Johansson, L. Sandhall, M. Sunemark, B. Smideberg, C. Olsson, and S. B. Olsson, "Non-invasive assessment of atrial refractoriness during atrial fibrillation in man—introducing, validating and illustrating a new ECG method," *Cardiovasc. Res.*, vol. 38, pp. 69–81, 1998.

[31] A. Bollmann, K. Sonne, H. Esperer, I. Toepffer, and H. Klein, "Circadian variations in atrial fibrillatory frequency in persistent human atrial fibrillation," *PACE*, vol. 23, pp. 1867–1871, 2000.

[32] C. Meurling *et al.*, "Dinural variations of the dominant cycle lenght of chronic atrial fibrillation," *Am. J. Physiol.*, vol. 280, pp. H401–H406, 2001.

[33] A. Bollmann, K. Wodarz, H. Esperer, I. Toepffer, and H. Klein, "Response of atrial fibrillatory activity to carotide sinus massage in patients with atrial fibrillation," *PACE*, vol. 24, pp. 1363–1368, 2001.

[34] M. Ingemansson, M. Holm, and S. B. Olsson, "Autonomic modulation of the atrial cycle length by the head up tilt test: non-invasive evaluation in patients with chronic atrial fibrillation," *Heart*, vol. 80, pp. 71–76, 1998.

[35] F. Nilsson, M. Stridh, A. Bollmann, and L. Sörnmo, "Predicting spontaneous termination of atrial fibrillation using the surface ECG," *Med. Eng. Physics*, vol. 28, pp. 802–808, 2006.

[36] A. Bollmann, N. Kanuru, K. McTeague, P. Walter, D. B. DeLurgio, and J. Langberg, "Frequency analysis of human atrial fibrillation using the surface electrocardiogram and its response to ibutilide," *Am. J. Cardiol.*, vol. 81, pp. 1439–1445, 1998.

[37] A. Bollmann, K. Binias, I. Toepffer, J. Molling, C. Geller, and H. Klein, "Importance of left atrial diameter and atrial fibrillatory frequency for conversion of persistent atrial fibrillation with oral flecainide," *Am. J. Cardiol.*, vol. 90, pp. 1011–1014, 2002.

[38] J. Langberg, J. Brunette, and K. McTeague, "Spectral analysis of the electrocardiogram predicts recurrence of atrial fibrillation after cardioversion," *J. Electrocardiol.*, vol. 31, pp. 80–84, 1998.

[39] M. Stridh, L. Sörnmo, C. J. Meurling, and S. B. Olsson, "Characterization of atrial fibrillation using the surface ECG: Time-dependent spectral properties," *IEEE Trans. Biomed. Eng.*, vol. 48, pp. 19–27, 2001.

[40] ——, "Sequential characterization of atrial tachyarrhythmias based on ECG time-frequency analysis," *IEEE Trans. Biomed. Eng.*, vol. 51, pp. 100–114, 2004.

[41] L. Rabiner and B. H. Juang, "An introduction to hidden Markov models," *IEEE ASSP Magazine*, pp. 4–19, 1986.

[42] R. L. Streit and R. F. Barrett, "Frequency line tracking using hidden Markov models," *IEEE Trans. Acoust., Speech, Signal Processing*, vol. 38, pp. 586–598, 1990.

Paper I

Paper I

Predicting Spontaneous Termination of Atrial Fibrillation Using the Surface ECG

Abstract

By recognizing and characterizing conditions under which atrial fibrillation (AF) is likely to terminate spontaneously or be sustained, improved treatment of sustained AF may result and unnecessary treatment of self-terminating AF avoided. Time-frequency measures that characterize AF, such as fibrillatory frequency, amplitude, and waveform shape (exponential decay), are extracted from the residual ECG following QRST cancellation. Three complexity measures are also studied, characterizing the degree of organization of atrial activity. All measures are analysed using a training set, consisting of 20 recordings of AF with known termination properties, and a test set of 30 recordings.

Spontaneous termination was best predicted by a low and stable fibrillatory frequency and a low exponential decay. Using these predictors, 90% of the test set was correctly classified into terminating and sustained AF. Neither fibrillation amplitude nor the complexity measures differed significantly between the two sets.

1   Introduction

Atrial fibrillation is the most common arrhythmia encountered in clinical practice with a prevalence of 0.4% of the general population and over 6% of people over 80 years old [1]. The treatment of AF patients is still unsatisfactory which, to a large extent, can be attributed to the progressing nature of this arrhythmia and high AF recurrence rates following restoration of sinus rhythm. Moreover, AF treatment, such as rate vs. rhythm control, choice of antiarrhythmic drugs or device therapy and curative ablation, is mostly done on a trial-and-error basis since current tests are neither able to predict the natural history of this arrhythmia nor its response to treatment. Consequently, current AF management guidelines do not provide treatment recommendations that "take the various mechanisms and patterns of AF into account" [1]. Therefore, it is desirable to develop tests which quantify AF disease state and guide AF management [2].

Atrial fibrillation can be subdivided into different forms, namely, (1) paroxysmal AF, i.e. self-terminating AF within 7 days, (2) persistent AF in which interventions are required for termination, and (3) permanent AF in which sinus rhythm cannot be restored or maintained. About 18% of paroxysmal AF evolve to permanent AF over 4 years [3]. Studying paroxysmal AF is important for several reasons. Firstly, identification of onset and termination mechanisms may lead to better pathophysiological understanding of the arrhythmia and, accordingly, more effective therapy. Secondly, by predicting spontaneous AF termination, unnecessary therapy may be avoided. In contrast, by predicting AF maintenance appropriate interventions may terminate the arrhythmia and prevent AF chronification. The aim of this work is to investigate the possibility to predict if and when an episode of atrial fibrillation terminates spontaneously.

When deriving a set of features for characterization of AF, the first step is to extract the atrial activity from the ECG signal. Various methods have been developed, e.g. blind source separation [4], principal component analysis [5] and spatiotemporal cancellation [6]. Spatiotemporal cancellation extends the well-known average beat subtraction technique [7] by using beat templates from adjacent leads in the cancellation process.

An important measure for ECG-based characterization is the fibrillatory frequency [5], shown to be strongly correlated with the invasively measured fibrillatory cycle length [8], [9]. Other measures are the amplitude and shape of the fibrillatory waves. The exponential decay is a recently presented parameter which characterizes the fibrillatory waves by the magnitudes of the fundamental frequency and its harmonics [10].

Entropy measures have previously been applied to study various types of biomedical signals [11], [12]. When studying atrial activity, entropy of the atrial activation process has been determined from the electrogram and suggested as a measure of AF organization [13]. Entropy measures based on the surface ECG have recently been suggested to distinguish AF from atrial flutter [14].

The paper is organized as follows: the measures derived from time-frequency analysis are described in Secs. 2.3–2.3 and the complexity measures in Sec. 2.4. Using the ECG database described in Sec. 3, the performances of the different measures are evaluated in Sec. 4.

2   Methods

Following baseline wander and 50 Hz filtering, the residual ECG is obtained by removing the QRST complexes using spatiotemporal cancellation. This cancellation technique is particularly well-suited for recordings with few leads such as those analysed in the present study. Details on QRST cancellation can be found in [6].

2.1   Log-spectral profile

The spectral properties of the AF waves are derived from the residual ECG using the method briefly summarized below [10]. Since the fibrillatory frequency changes over time, it is necessary to use a time-dependent frequency analysis method such as the short-time Fourier transform. The residual ECG signal, $x(n)$, is divided into overlapping segments of length N. The l:th segment, denoted $\mathbf{x}_l$, is defined as

$$\mathbf{x}_l = \begin{bmatrix} x(lL) \\ x(lL+1) \\ \vdots \\ x(lL+N-1) \end{bmatrix}, \tag{1}$$

where L is the distance between consecutive segments. The spectrum, $\mathbf{q}_l$, of each segment is calculated as

$$\mathbf{q}_l = \mathbf{F}\mathbf{W}\mathbf{x}_l, \tag{2}$$

where the $K \times N$ matrix $\mathbf{F}$ defines the K-point discrete, nonuniform Fourier transform, and the elements of the $N \times N$ diagonal matrix $\mathbf{W}$ defines a window function. The transform matrix $\mathbf{F}$ is defined by

$$\mathbf{F} = \begin{bmatrix} \mathbf{1} & e^{-j2\pi\mathbf{f}} & e^{-j2\pi\mathbf{f}2} & \cdots & e^{-j2\pi\mathbf{f}(N-1)} \end{bmatrix}, \tag{3}$$

where $\mathbf{f} = [f_0 \cdots f_{K-1}]^T$ is a logarithmically scaled frequency vector, with

$$f_k = f_0 \cdot 10^{\frac{k}{K}}, \quad k = 0, \ldots, K-1. \tag{4}$$

Since the phase of the spectrum is ignored, $\mathbf{q}_l$ is redefined such that

$$|\mathbf{q}_l| \rightarrow \mathbf{q}_l. \tag{5}$$

Each observed spectrum $\mathbf{q}_l$ can be modeled by $\tilde{\mathbf{q}}_l$ being a frequency-shifted, θ_l, and amplitude-scaled, a_l,version of a known real-valued spectral profile, ϕ_l,

$$\tilde{\mathbf{q}}_l = a_l\, \mathbf{J}_{\theta_l}\, \phi_l, \tag{6}$$

where the matrix $\mathbf{J}_{\theta_l}$ performs the frequency shift by selecting the appropriate interval of ϕ_l. The amplitude parameter a_l and the frequency-shift parameter θ_l can be estimated by minimizing the quadratic cost function, $J(\theta_l, a_l)$, so that the model, $\tilde{\mathbf{q}}_l$, optimally matches the true spectrum, $\mathbf{q}_l$,

$$J(\theta_l, a_l) = (\mathbf{q}_l - \tilde{\mathbf{q}}_l)^T \mathbf{D} (\mathbf{q}_l - \tilde{\mathbf{q}}_l) \tag{7}$$

$$= (\mathbf{q}_l - a_l\mathbf{J}_{\theta_l}\phi_l)^T \mathbf{D} (\mathbf{q}_l - a_l\mathbf{J}_{\theta_l}\phi_l), \tag{8}$$

where $\mathbf{D}$ is a $K \times K$ diagonal matrix designed to weight the error of the frequency components differently. For compensation of the logarithmic frequency scaling, the diagonal elements, d_k, of matrix $\mathbf{D}$ are set to

$$d_k = \frac{Nf_0}{f_s} \left(10^{\frac{k}{K}} - 10^{\frac{k-1}{K}} \right). \tag{9}$$

Minimization of (8) results in an estimator of the frequency-shift [10],

$$\hat{\theta}_l = \arg\max_{\theta_l} \left[\mathbf{q}_l^T \mathbf{D}^{\frac{1}{2}} \mathbf{J}_{\theta_l} \mathbf{D}^{\frac{1}{2}} \phi_l \right], \tag{10}$$
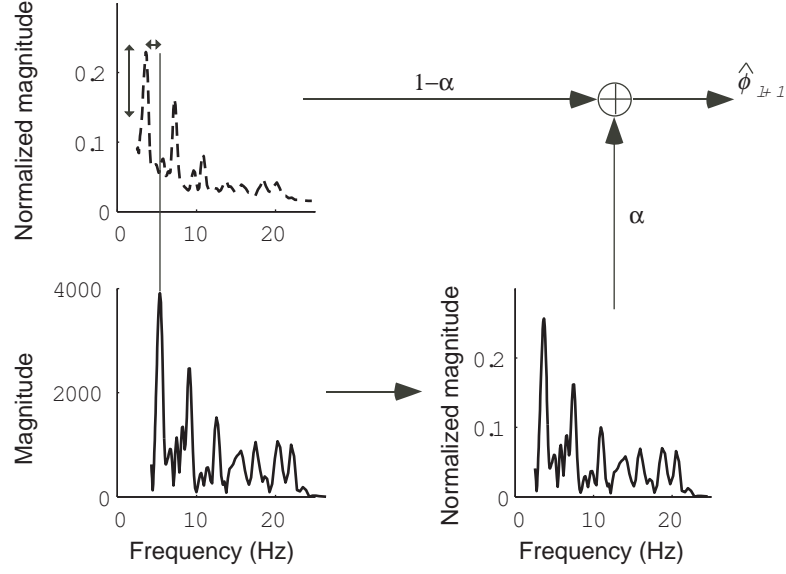
Figure 1: The spectral profile ϕ_l (top) is frequency-shifted and amplitude-scaled, as marked by the small arrows, to best model the spectrum $\mathbf{q}_l$ (bottom left). The spectral profile is then updated by the inversely frequency-shifted and amplitude-scaled version of $\mathbf{q}_l$ (bottom right).

and an estimator of the amplitude,

$$\hat{a}_l = \mathbf{q}_l^T \mathbf{D}^{\frac{1}{2}} \mathbf{J}_{\hat{\theta}_l} \mathbf{D}^{\frac{1}{2}} \boldsymbol{\phi}_l. \tag{11}$$

With estimates of a_l and θ_l, we obtain

$$\hat{\mathbf{q}}_l = \hat{a}_l \, \mathbf{J}_{\hat{\theta}_l} \, \phi_l. \tag{12}$$

The model error, normalized with respect to the amplitude estimate, is given by

$$e_l = \frac{1}{\hat{a}_l^2} J(\hat{\theta}_l, \hat{a}_l) = \frac{1}{\hat{a}_l^2} (\mathbf{q}_l - \hat{\mathbf{q}}_l)^T \mathbf{D} \, (\mathbf{q}_l - \hat{\mathbf{q}}_l). \tag{13}$$

For the first segment, the spectral profile, ϕ_0, is initiated by

$$\boldsymbol{\phi}_0 \quad = \quad \begin{bmatrix} 0.01 & \cdots & 0.01 & 1 & 0.01 & \cdots & 0.01 \end{bmatrix}^T, \tag{14}$$

where ϕ_0 is 1 at the peak position and 0.01 at all other positions. The spectral profile, ϕ_l, is then updated for each segment through exponential averaging so that

$$\hat{\phi}_{l+1} = (1 - \alpha_l)\hat{\phi}_l + \alpha_l \frac{\mathbf{J}_{\hat{\theta}_l} \hat{\mathbf{q}}_l}{\|\mathbf{J}_{\hat{\theta}_l} \hat{\mathbf{q}}_l\|}, \quad l > 0, \tag{15}$$

where the gain α_l $(0 < \alpha_l < 1)$ is set to a positive value when the signal is judged reliable (see Sec 2.3), and otherwise zero. Figure 1 illustrates the fitting and updating of the spectral profile, ϕ_l, to the observed spectrum, $\mathbf{q}_l$.

2.2 Time-frequency measures

The *fibrillatory frequency*, $\hat{f}_l$, corresponds to the location of the dominant peak of the residual ECG spectrum, $\mathbf{q}_l$. In this case, the fibrillatory frequency corresponds to the peak frequency of the spectral profile, compensated with the frequency shift, $\hat{\theta}_l$. The *fibrillation amplitude* is the amplitude scaling, $\hat{a}_l$, of the spectral profile. Since the spectral profile is normalized, this measure is related to the effective amplitude of the fibrillatory waves. Wave shape is characterized by the fundamental and harmonics of the spectral profile. A spectral line model is used to parameterize the shape by means of the magnitude of the spectral profile, ϕ_l, at its harmonics, defined by

$$\phi_l(p_l + h_m) = \begin{cases} b_l e^{-\gamma_l m}, & m = 0, 1, \ldots, M \\ 0, & \text{otherwise,} \end{cases} \tag{16}$$

where b_l is the peak magnitude of the fundamental frequency, and γ_l is the exponential decay of the M harmonics; M is here chosen so that only harmonics below 20 Hz are used. The parameter h_m denotes the offset position of the m:th harmonic in relation to the fundamental frequency at p_l. The offset position is independent of the fundamental frequency since logarithmic scaling is used. The *exponential decay*, γ_l, and the peak magnitude, b_l, are estimated by minimizing the least squares cost function using the logarithm of the spectral line model,

$$J(\ln b_l, \gamma_l) = \sum_{m=0}^{M} (\ln \phi_l(p_l + h_m) - (\ln b_l - \gamma_l m))^2. \tag{17}$$

The resulting estimator of the exponential decay, $\hat{\gamma}_l$, is given by

$$\hat{\gamma}_l = \frac{6}{M'(M'+1)} \sum_{m=0}^{M} (\ln \phi_l(p_l + h_m) + \frac{12}{M'((M')^2 - 1)} \sum_{m+1}^{M} m \ln \phi_l(p_l + h_m), \tag{18}$$

where $M' = M + 1$.

The parameter estimates $\hat{f}_l$, $\hat{a}_l$, and $\hat{\gamma}_l$ are obtained for each frame of 128 samples (i.e. 2.56 seconds at a sampling rate of 50 Hz). From the resulting series of estimates the mean and standard deviation can be determined for the recording.

2.3 Validity

In situations when the residual ECG signal is extremely noisy and/or occasional episodes of sinus rhythm are included, it is necessary to exclude segments not containing atrial tachyarrhythmia. In order to determine if the l:th segment contains AF, four measures based on ϕ_l are employed, namely, the signal-to-noise-ratio (SNR), the second peak position (SPP), the second peak amplitude (SPA), and the model error ϵ, defined as the difference between the true spectrum, $\mathbf{q}_l$, and the fitted spectral profile, $\tilde{\mathbf{q}}_l$,

$$\epsilon_l = |\mathbf{q}_l - \tilde{\mathbf{q}}_l|. \tag{19}$$

The SNR is defined as the ratio between the mean of the fundamental and first harmonic magnitudes, denoted $\phi_l(p_0(l))$ and $\phi_l(p_1(l))$, respectively, and the magnitude of the background noise, $\phi_l(p_b(l))$,

$$z_{SNR}(l) = \frac{(\phi_l(p_0(l)) + \phi_l(p_1(l)))/2}{\phi_l(p_b(l))}. \tag{20}$$

The SPP is defined as the ratio between the distance from the fundamental frequency, $p_0(l)$, to the second largest peak, $p_s(l)$, and the distance from the fundamental frequency to the first harmonic, $p_1(l)$,

$$z_{SPP}(l) = \left| \frac{p_0(l) - p_s(l)}{p_0(l) - p_1(l)} \right|. \tag{21}$$

The SPA is defined as the ratio between the magnitude of the second peak, $\phi_l(p_s(l))$, and the magnitude of the fundamental peak, $\phi_l(p_0(l))$,

$$z_{SPA}(l) = \frac{\phi_l(p_s(l))}{\phi_l(p_0(l))}. \tag{22}$$

The ECG signal segment is considered to contain atrial activity if 1) the SNR is sufficiently large, 2) the model error exhibits no sudden decrease, 3) the second largest peak has neither too high a magnitude nor 4) is too close to the position of the fundamental frequency [15].

When occasional episodes of sinus rhythm and local noise have been excluded by the validity parameters, the time-frequency measures of the remaining segments are averaged producing reliable averages of the fibrillatory frequency, $\bar{f}$, the exponential decay, $\bar{\gamma}$, and the peak amplitude, $\bar{a}$. The variation of the fibrillatory frequency, σ_f, is described by the standard deviation of the fibrillatory frequency. If more than 75% of the signal segments are invalid, the entire recording is excluded from further analysis.

2.4   Complexity measures

Three different measures are investigated for the purpose of characterizing AF complexity, namely, spectral entropy, sample entropy, and fractional spectral radius. The *spectral entropy*, $\mathcal{H}_{SpE}$, quantifies the spectral complexity of a signal, $x(n)$, and is obtained by applying Shannon's entropy to the probability density function (PDF) of the signal [11],

$$\mathcal{H}_{SpE} = \sum_f p_f \log \frac{1}{p_f} \tag{23}$$

where p_f is the value of the PDF at bin f. A high value of $\mathcal{H}_{SpE}$ indicates high complexity of $x(n)$. In our case the PDF is "approximated" by the area-normalized power spectral density obtained from the 256-point Fourier transform. A value of $\mathcal{H}_{SpE}$ is calculated for every non-overlapping Hanning-windowed segment of 100 samples from $x(n)$, i.e. 2 seconds at a sampling rate of 50 Hz.

The *sample entropy*, $\mathcal{H}_{SaE}$, compares similarity in fixed length segments of the signal [12]. The signal $x(n)$ is divided into different time segments, $\mathbf{x}_m(i)$, of length m, starting at time index i,

$$\mathbf{x}_m(i) = \begin{bmatrix} x(i) & x(i+1) & \cdots & x(i+m-1) \end{bmatrix}^T. \tag{24}$$

The distance between two vectors, $\mathbf{x}_m(i)$ and $\mathbf{x}_m(j)$, is calculated as the infinity norm,

$$d(\mathbf{x}_m(i), \mathbf{x}_m(j)) = \max\left(|\mathbf{x}_m(i) - \mathbf{x}_m(j)|\right). \tag{25}$$

The number of vectors $\mathbf{x}_m(j)$ within the distance r of vector $\mathbf{x}_m(i)$, $j \neq i$, is denoted A_i. Then, $D_i^m(r)$ represents an estimate of the probability that any segment of length m in the signal is similar to the vector $\mathbf{x}_m(i)$,

$$D_i^m(r) = \frac{A_i^m}{N - m - 1}, \tag{26}$$

and $D^m(r)$ is the probability that any pair of two vectors of length m are similar,

$$D^m(r) = \frac{\sum_{i=0}^{N-m-1} D_i^m(r)}{N - m}. \tag{27}$$

The sample entropy, $\mathcal{H}_{SaE}$, is defined as

$$\mathcal{H}_{SaE}(m, r, N) = -\ln\left(\frac{D^{m+1}(r)}{D^m(r)}\right). \tag{28}$$

A high value of $\mathcal{H}_{SaE}$ indicates high complexity of $x(n)$. The length of $x(n)$, denoted N, is in the present study 100 samples, i.e. 2 seconds at a sampling rate of 50 Hz. The distance, r, is set to 0.2 times the standard deviation of $x(n)$, and m is set to 1.

The *fractional spectral radius*, $\mathcal{H}_{FSR}$, is another measure of complexity which gives an upper bound to the trajectory dimension [11]. The signal, $x(n)$, is divided into different time segments, $\mathbf{x}_m(i)$, as previously defined in (24). The time segment vectors $\mathbf{x}_m(i)$ are placed in a matrix, $\mathbf{X}_m$.

$$\mathbf{X}_m \quad = \quad \begin{bmatrix} \mathbf{x}_m(1) & \mathbf{x}_m(2) & \cdots & \mathbf{x}_m(N-m) \end{bmatrix}. \tag{29}$$

The autocorrelation matrix $\mathbf{U}$ of $\mathbf{X}_m$ is then obtained as

$$\mathbf{U} = \mathbf{X}_m^T \mathbf{X}_m, \tag{30}$$

whose eigenvalues are denoted σ_i^2, $\sigma_1^2 > \sigma_2^2 > \cdots > \sigma_m^2$. The fractional spectral radius, $\mathcal{H}_{FSR}$, is the ratio between the sum of the j largest eigenvalues and the total sum of eigenvalues.

$$\mathcal{H}_{FSR}(j) = \frac{\sum_{i=1}^{j} \sigma_i^2}{\sum_{l=0}^{m} \sigma_l^2} \tag{31}$$

A small value of $\mathcal{H}_{FSR}$ indicates a large trajectory dimension, and hence high complexity of $x(n)$. A value of $\mathcal{H}_{FSR}$ is calculated for every 200 samples, i.e. 4 seconds at a sampling rate of 50 Hz, of the signal $x(n)$. The segment size, m, is set to 100 samples, and only the largest eigenvalue is considered, i.e. $j = 1$.

3   Database

The database was provided by Physionet [16] for the Computers in Cardiology Challenge 2004, and consists of 80 two-channel ECG recordings. One minute segments were extracted from 20–24 hours Holter recordings from patients with paroxysmal AF (sampling rate of 128 Hz, 16 bits/sample, $5\mu V$ resolution). The recordings were divided into a training set and two test sets (A and B). The training set contains 30 recordings, labeled either non-terminating (N), immediately-terminating (T), or soon-terminating (S). Ten recordings are labeled N, meaning that the AF episode continues at least one hour after the end of the recording. Twenty recordings from ten different patients are labeled S or T, where T recordings immediately follow S recordings. The AF episode terminates within one second of the end of the T recording, and consequently one minute after the end of the S recording.

Test set A contains 30 recordings from the same number of patients. The labels of the recordings are concealed, but it is known that approximately half are labeled N and half T. Test set B contains 20 recordings, one labeled S and one labeled T from each of ten patients. The patient number and labels of the 20 recordings are concealed.

Following QRST cancellation, the signals are resampled to 50 Hz, and the ECG lead with most valid segments is considered for further analysis. In one of the signals in the training set (6N) more than 75% of the segments were considered invalid because of noise and poor QRST cancellation and, therefore, the entire signal was excluded from analysis.

4   Results

The mean and standard deviation of each measure among the non-terminating (N) and the terminating (T) AF recordings of the training set are shown in Table 1. A two-sample Kolmogorov-Smirnov goodness-of-fit hypothesis test was employed to determine whether there were any differences in the measures from N and T recordings. The fibrillatory frequency, $\bar{f}$, the exponential decay, $\bar{\gamma}$, and the

Table 1: Mean value and standard deviation of measures used for AF characterization, for the non-terminating (N) and immediately-terminating (T) signals in the training set. Measures with boldface asymptotic p-values are significantly different according to a Kolmogorov-Smirnov test.

Parameter average	N $Mean \pm Std$	T $Mean \pm Std$	Asymptotic p-value
f	6.91 ± 0.66	5.00 ± 0.65	**0.000033**
$\bar{\gamma}$	1.29 ± 0.27	0.79 ± 0.20	**0.0021**
σ_f	0.80 ± 0.23	0.52 ± 0.13	**0.0127**
$\bar{a}$	21.7 ± 12.4	28.6 ± 16.7	N.S.
$\mathcal{H}_{SpE}$	1.73 ± 0.34	1.73 ± 0.18	N.S.
$\mathcal{H}_{SaE}$	1.51 ± 0.34	1.63 ± 0.16	N.S.
$\mathcal{H}_{FSR}$	0.16 ± 0.04	0.14 ± 0.02	N.S.

Table 2: Mean value and standard deviation of measures used for AF characterization, from the soon-terminating (S) and immediately-terminating (T) signals in the training set.

Parameter average	S $Mean \pm Std$	T $Mean \pm Std$	Asymptotic p-value
f	5.33 ± 0.65	5.00 ± 0.65	N.S.
$\bar{\gamma}$	0.90 ± 0.17	0.79 ± 0.20	N.S.
σ_f	0.67 ± 0.32	0.52 ± 0.13	N.S.
$\bar{a}$	32.3 ± 17.8	28.6 ± 16.7	N.S.
$SpecEn$	1.74 ± 0.16	1.73 ± 0.18	N.S.
$SampEn$	1.61 ± 0.12	1.63 ± 0.16	N.S.
FSR	0.16 ± 0.03	0.14 ± 0.02	N.S.

variation of the fibrillatory frequency, σ_f, differ significantly between non-terminating and terminating AF as implied by the asymptotic p-value. Neither the peak amplitude, $\bar{a}$, nor the complexity measures ($\mathcal{H}_{SpE}$, $\mathcal{H}_{SaE}$ and $\mathcal{H}_{FSR}$) could distinguish between the two AF categories.

There were no significant differences between any of the measures obtained from the soon-terminating (S) and the immediately-terminating (T) signals of the training set, as shown in Table 2.

Studying the residual ECG signals of the training set, we found that terminating AF generally exhibits a lower fibrillatory frequency. The fibrillatory waves are generally more regular, which results in a smaller variation of the fibrillatory frequency, σ_f. They have lower exponential decay of the harmonics, γ, than waves of non-terminating AF, see Figure 2. The peak amplitude is usually slightly larger in terminating AF than in non-terminating AF, however, the difference is not significant.

Since there is considerable correlation between f and γ ($r = 0.9$, $p < 0.0001$), γ and σ_f ($r = 0.7$, $p < 0.005$), and f and σ_f ($r = 0.5$, $p < 0.05$), only the most significant measure, i.e. the fibrillatory frequency f, was used for classification. The recordings of the training set and test set A were classified as non-terminating (N) if their average fibrillatory frequency exceeded 5.7 Hz, and terminating (T) AF otherwise. The classification results are presented in Table 3.
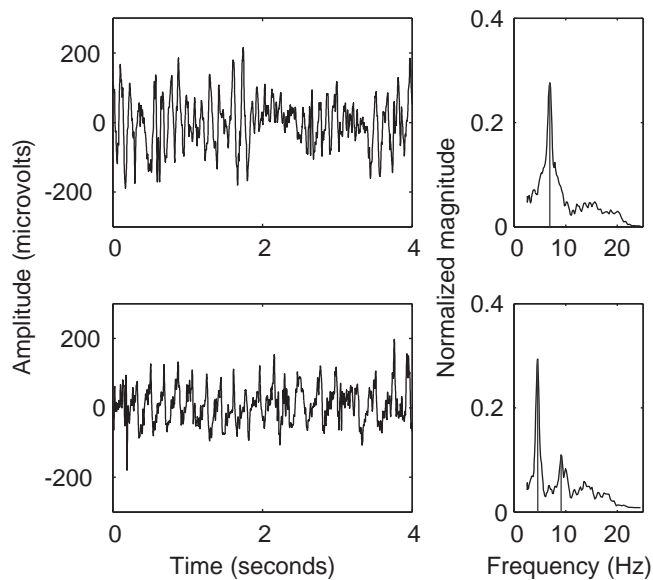
Figure 2: Residual ECGs (left) with different exponential decay, $\bar{\gamma}$, fibrillatory frequency, $\bar{f}$, and variation of fibrillatory frequency, σ_f and corresponding spectral profile, ϕ_l (right). (a) Non-terminating AF with $\bar{\gamma} = 1.6$, $\bar{f} = 7.6$ Hz and $\sigma_f = 0.9$, and (b) terminating AF with $\bar{\gamma} = 0.7$, $\bar{f} = 5.0$ Hz, $\sigma_f = 0.4$.

Table 3: Classification into non-terminating (N) and terminating (T) AF for the recordings of the training set and test set.

	N/T
Training set	**19/20**
Test set	**27/30**

5   Discussion

The present study shows that classification of ECG signals into terminating and non-terminating paroxysmal AF based on their fibrillatory frequency works well. Since the three significant measures, i.e., fibrillatory frequency, exponential decay and variation of fibrillatory frequency, were highly correlated, only the most significant measure was used for classification. Restricting the classification to only one measure is also motivated by the small size of the database. However, multivariate classification involving measures such as exponential decay may improve the performance when larger databases are analysed.

The idea that fibrillatory frequency predicts spontaneous [8], [17] or drug-induced AF termination [8], [18] has previously been advocated by our group. In a comparable study using Holter recordings with paroxysmal AF, Bollmann et al. found a lower fibrillatory frequency in episodes lasting less than 15 minutes than in longer episodes. In longer episodes, the fibrillatory frequency increased during the first 5 minutes after AF onset and decreased in the last minute prior to AF termination [17].

Table 2 suggests that negligible differences exist between the S and T recordings of the training set. This result is expected since the recordings are consecutive from the same patients. A dynamic analysis was presented in [19] for the purpose of distinguishing S from T recordings, where the measures were computed from the last segment, i.e., the last 2.5 seconds, and compared. The fibrillatory frequency was found to be slightly lower in T recordings than in S recordings during the last seconds. However, this difference was not statistically significant (using a Kolmogorov-Smirnov test) since the difference among different recordings was substantial. In another step, we compared the measurements of the last segment in the S and T recordings from the same patient, and the results showed that the fibrillatory frequency was significantly lower in the T recording than in the S recording [19].

Since an AF episode is more likely to terminate spontaneously when fibrillatory frequency is lower, recordings from one patient may be classified into soon-terminating and immediately-terminating based on fibrillatory frequency of the last seconds in the recording; a finding which agrees with the result that an abrupt decrease in fibrillatory frequency is observed in right atrial electrograms 1Ð2 seconds before spontaneous AF termination [20]. However, the fibrillatory frequency did not, in general, attain its minimum value at the end of the recordings of the present database [19] and, therefore, prediction of when an AF episode terminates remains difficult to perform accurately with current techniques. Moreover, from a therapeutic point of view prediction of the exact termination timing within one second is not warranted.

Various complexity measures have previously been applied to characterize organization of the atrial activation time series, obtained from atrial electrograms [21], [13]. Such atrial activation complexity measures differ from the complexity measures investigated in this study whose aim are to quantify complexity of atrial waveforms using the surface ECG signal. Waveform complexity measures have previously been applied to ECG signals for discrimination of AF and atrial flutter [14]. The complexity measures applied to residual ECG signals in this study have previously been applied to EEG signals in order to characterize differing depth of anesthesia [11]. However, none of the complexity measures investigated were capable of distinguishing terminating from non-terminating AF in the two-lead Holter recordings. Poor SNR is believed to be the main reason to this negative result; the complexity measures may perform better on ECG signals with higher SNRs.

6   Conclusions

Predicting patients prone to spontaneous AF termination from Holter ECG recordings can be done with good accuracy (90%). A low and stable fibrillatory frequency and a low exponential decay of

the spectral profile are good indicators of spontaneous termination. To produce reliable estimates of these measures, the robustness of the present time-frequency analysis method is crucial when analysing noisy signals.

References

[1] V. Fuster *et al.*, "ACC/AHA/ESC guidelines for the management of patients with atrial fibrillation," *Circ.*, vol. 104, pp. 2118–2150, 2001.

[2] A. Bollmann, "Quantification of electrical remodeling in human atrial fibrillation," *Cardiovasc. Res.*, vol. 47, pp. 207–209, 2000.

[3] S. Al-Khatib, W. Wilkinson, L. Sanders, E. McCarthy, and E. Pritchett, "Observations on the transition from intermittent to permanent atrial fibrillation," *Am. Heart J.*, vol. 140, pp. 142–145, 2000.

[4] J. J. Rieta, V. Zarzoso, J. Millet-Roig, R. Garcia-Civera, and R. Ruiz-Granell, "Atrial activity extraction based on blind source separation as an alternative QRST cancellation for atrial fibrillation analysis," in *Proc. Computers in Cardiology*. IEEE Press, 2000, pp. 69–72.

[5] P. Langley, J. P. Bourke, and A. Murray, "Frequency analysis of atrial fibrillation," in *Proc. Computers in Cardiology*. IEEE Press, 2000, pp. 65–68.

[6] M. Stridh and L. Sörnmo, "Spatiotemporal QRST cancellation techniques for analysis of atrial fibrillation," *IEEE Trans. Biomed. Eng.*, vol. 48, pp. 105–111, 2001.

[7] J. Slocum, E. Byrom, L. McCarthy, A. Sahakian, and S. Swiryn, "Computer detection of atrioventricular dissociation from surface electrocardiograms during wide QRS complex tachycardia," *Circ.*, vol. 72, pp. 1028–1036, 1985.

[8] A. Bollmann, N. Kanuru, K. McTeague, P. Walter, D. B. DeLurgio, and J. Langberg, "Frequency analysis of human atrial fibrillation using the surface electrocardiogram and its response to ibutilide," *Am. J. Cardiol.*, vol. 81, pp. 1439–1445, 1998.

[9] M. Holm, S. Pehrsson, M. Ingemansson, L. Sörnmo, R. Johansson, L. Sandhall, M. Sunemark, B. Smideberg, C. Olsson, and S. B. Olsson, "Non-invasive assessment of atrial refractoriness during atrial fibrillation in man—introducing, validating and illustrating a new ECG method," *Cardiovasc. Res.*, vol. 38, pp. 69–81, 1998.

[10] M. Stridh, L. Sörnmo, C. J. Meurling, and S. B. Olsson, "Sequential characterization of atrial tachyarrhythmias based on ECG time-frequency analysis," *IEEE Trans. Biomed. Eng.*, vol. 51, pp. 100–114, 2004.

[11] I. A. Rezek and S. J. Roberts, "Stochastic complexity measures for physiological signal analysis," *IEEE Trans. Biomed. Eng.*, vol. 45, pp. 1186–1191, 1998.

[12] S. J. Richman and J. R. Moorman, "Physiological time-series analysis using approximate entropy and sample entropy," *Am. J. Physiol.*, vol. 278, pp. H2039–H2049, 2000.

[13] F. Censi, V. Barbaro, P. Bartolini, G. Calcagnini, A. Michelucci, and S. Cerutti, "Non-linear coupling of atrial activation processes during atrial fibrillation in humans," *Biol. Cybern.*, vol. 85, pp. 195–201, 2001.

[14] Y. Su, T. Kao, H. Tso, Y. Lin, S. Chen, and C. Tai, "Nonlinear analysis of human atrial flutter and fibrillation using the surface electrocardiogram," *Computers in Cardiology*, vol. 31, pp. 441–444, 2004.

[15] M. Stridh, L. Sörnmo, and S. B. Olsson, "ECG-based feature tracking in atrial tachyarrhythmias," *Computers in Cardiology*, vol. 30, pp. 721–724, 2003.

[16] A. L. Goldberger, L. A. N. Amaral, L. Glass, J. M. Hausdorff, P. C. Ivanov, R. G. Mark, J. E. Mietus, G. B. Moody, C.-K. Peng, and H. E. Stanley, "PhysioBank, PhysioToolkit, and PhysioNet: Components of a new research resource for complex physiologic signals," *Circ.*, vol. 101, pp. e215–e220, 2000.

[17] A. Bollmann, K. Sonne, H. Esperer, I. Toepffer, J. Langberg, and H. Klein, "Non-invasive assessment of fibrillatory activity in patients with paroxysmal and persistent atrial fibrillation using the Holter ECG," *Cardiovasc. Res.*, vol. 44, pp. 60–66, 1999.

[18] A. Bollmann, K. Binias, I. Toepffer, J. Molling, C. Geller, and H. Klein, "Importance of left atrial diameter and atrial fibrillatory frequency for conversion of persistent atrial fibrillation with oral flecainide," *Am. J. Cardiol.*, vol. 90, pp. 1011–1014, 2002.

[19] F. Nilsson, M. Stridh, A. Bollmann, and L. Sörnmo, "Predicting spontaneous termination of atrial fibrillation with time-frequency information," *Computers in Cardiology*, vol. 31, pp. 657–660, 2004.

[20] A. Bollmann and J. Langberg, "Spectral analysis of atrial electrograms predicts spontaneous termination of atrial fibrillation," *Pacing Clin. Electrophysiol.*, p. 979, 1998.

[21] L. Mainardi, G. Calcagnini, A. Porta, F. Censi, P. Bartolini, and S. Cerutti, "Linear and non-linear parameters for the classification of atrial fibrillation episodes from intra-atrial signals," *Computers in Cardiology*, vol. 26, pp. 691–694, 1999.

Paper II

Paper II

Frequency Tracking of Atrial Fibrillation using Hidden Markov Models

Abstract

A Hidden Markov Model (HMM) is employed to improve noise robustness when tracking the dominant frequency of atrial fibrillation (AF) in the ECG. Following QRST cancellation, a sequence of observed frequency states is obtained from the residual ECG, using the short-time Fourier transform. Based on the observed state sequence, the Viterbi algorithm retrieves the optimal state sequence by exploiting the state transition matrix, incorporating knowledge on AF characteristics, and the observation matrix, incorporating knowledge of the frequency estimation method and SNR. The tracking method is evaluated with simulated AF signals to which noise, obtained from ECG recordings, has been added at different SNRs. The results show that the use of HMM improves performance considerably by reducing the RMS error associated with frequency tracking: at 4 dB SNR the RMS error drops from 0.2 Hz to 0.04 Hz.

1 Introduction

Atrial fibrillation (AF) is a common arrhythmia, with a prevalence of over 6% for people over 80 years old [1]. The arrhythmia can be studied through the atrial activity of the surface ECG, manifested by fibrillation waves. The repetition rate of the fibrillation waves—the AF frequency—plays an important role when analyzing atrial fibrillation from the ECG. Several studies have demonstrated significant correlation between AF frequency and the likelihood of spontaneous or drug-induced AF termination, where a lower AF frequency indicates a higher likelihood of termination [2–5].

To study the spectral properties of atrial activity, it is necessary to first cancel the ventricular activity, i.e., the QRST complexes. This task can be accomplished using a range of methods, including average beat subtraction methods such as spatiotemporal cancellation [6], and source separation methods such as principal component analysis [7] and blind source separation [8]. The extracted atrial activity is here referred to as the residual ECG.

The AF frequency has usually been determined from the periodogram of the residual ECG, thus precluding the detection of changes in AF frequency. Such changes can be tracked by employing the short-time Fourier transform (STFT), however, that approach suffers from vulnerability to noise. A more robust approach was recently presented in which AF frequency is tracked through least squares fitting of a template spectrum to individual spectral slices [9]. In that approach, the time-frequency distribution of the AF signal is calculated using a logarithmically scaled short-time Fourier transform. Each short-time spectrum is fitted to the spectral template, by amplitude scaling and frequency shifting, including the fundamental frequency and harmonics up to 20 Hz. The spectral template is updated through exponential averaging. The frequency shifted peak of the spectral template gives a more robust estimate of the AF frequency than STFT peak detection, and offers better time resolution than the periodogram. Nonetheless, the residual ECG is sometimes corrupted by noise due to muscular activity or insufficient QRST cancellation which cause the AF frequency estimate to become inaccurate.

A structured approach to handle this problem is to use a Hidden Markov Model (HMM) for frequency tracking. With an HMM, short-time frequency estimates that differ significantly from the frequency trend can be detected and excluded or replaced by estimates based on adjacent frequencies. A Markov model consists of a finite number of states with predefined state transition probabilities. The likelihood of a certain state, corresponding to a unique set of observed variables, depends only on the previous state (random walk). In an HMM the state variables cannot be directly observed, but each state is associated with certain observation probabilities, i.e., the probabilities of observing a specific set of variables. Given the observation sequence of an HMM, the optimal state sequence can be obtained using the Viterbi algorithm or the Forward-Backward algorithm.

An HMM is well-suited for frequency tracking of a signal. The states of the model correspond to the underlying frequencies, while the observations are determined by the estimated frequency of a specific time interval of the signal. A priori knowledge on the likelihood with which the AF frequency changes is included in the state transition probabilities, whereas knowledge about the frequency estimation method and SNR are included in the observation probabilities.

Hidden Markov models have previously been applied in various radar and sonar applications where it is of interest to track sinusoids embedded in noise. HMM-based methods for frequency tracking have been presented for a single sinusoid [10] as well as for two independent sinusoids [11, 12]. Several attempts have been made to improve frequency tracking by including additional information in observation vector of the HMM such as the magnitude and phase of the detected frequency [13] and the entire periodogram of the measured signal [14]. Another approach is to include information on the rate of frequency change in the state vector [14].

The purpose of this study is to investigate the suitability of HMMs for AF frequency tracking in ECG signals. Since an AF spectrum can be harmonic, the HMM is extended from the common single sinusoid-in-noise model (Sec. 2.1) to also account for the presence of harmonics (to our knowledge,

the derivation is novel to this paper, see Sec. 2.2). The performance of the present method for AF frequency tracking is compared to that of the STFT and the spectral template method, using simulated AF signals mixed with noise obtained from ECG recordings (Sec. 3). The results are presented in Sec. 4.

2   Methods

Certain assumptions on the AF signal need to be introduced when employing an HMM for frequency tracking. It is assumed that changes in AF frequency are characterized by a Gaussian probability density function, i.e., the AF frequency is more probable to remain the same or change gradually than to change drastically. Another assumption is that the AF frequency remains constant during the time interval in which the Fourier transform is calculated. Yet another assumption is that the AF signal can be modeled as a sinusoidal signal corrupted with additive white noise.

2.1   A Hidden Markov Model for Single Frequency Tracking

Given an observed sequence of frequency estimates, $\mathbf{z} = [z(1), z(2), \ldots, z(T)]^T$, our goal is to obtain the true sequence, denoted $\mathbf{x} = [x(1), x(2), \ldots, x(T)]^T$. The HMM for frequency tracking includes one zero state, $z(t) = 0$, when no signal is present, and $P - 1$ different frequency states, $z(t) = 1, \ldots, P - 1$, where state i includes frequencies between f_i and $f_{i+1} = f_i + \Delta f$, with a center frequency of $\tilde{f}_i$,

$$\tilde{f}_i = f_i + \frac{\Delta f}{2}. \tag{1}$$

The HMM is completely characterized by a state transition matrix $\mathbf{A}$, an observation matrix $\mathbf{B}$, and an initial state vector $\boldsymbol{\pi}$ [15].

State transition matrix

The $P \times P$ state transition matrix $\mathbf{A}$ describes the transition probabilities between different states. Element a_{ij} is the probability that state $x(t + 1) = j$ if state $x(t) = i$. Each row must sum to unity since the elements of a row correspond to the transition probabilities of a certain state. The probability of track initialization in state $j \neq 0$, a_{0j}, is identical for all frequency states,

$$a_{0j} = \frac{u}{P - 1}, \quad j = 1, 2, \ldots, P - 1. \tag{2}$$

Hence, the probability for remaining in the zero state, a_{00}, i.e., when no signal is present, is

$$a_{00} = 1 - u. \tag{3}$$

The probability of track termination, a_{j0}, is equal for all frequency states,

$$a_{j0} = v, \quad j = 1, 2, \ldots, P - 1. \tag{4}$$

The transition probability $\tilde{a}_{ij}$ between the non-zero states is set to

$$\tilde{a}_{ij} = \frac{(1 - v)g_{ij}}{\sum_{k=1}^{P} g_{ik}}, \quad i, j = 1, 2, \ldots, P - 1, \tag{5}$$

where

$$g_{ij} = \frac{1}{d\sqrt{2\pi}} \int_{f_j}^{f_j + \Delta f} \exp\left[-\frac{(f - \tilde{f}_i)^2}{2d^2} \right] df \tag{6}$$

since the location of the frequency track at the next time instant is assumed to be Gaussian with mean $\tilde{f}_i$ and standard deviation d. This assumption results in an unbalanced $\mathbf{A}$, since the diagonal elements of a_{ii} depend on state i. Hence, all diagonal elements are set to the smallest diagonal element,

$$a_{min} = \min_{1 \leq i \leq P-1} \tilde{a}_{ii}. \tag{7}$$

Consequently, the other $P-1$ elements of the row need to be adjusted so that the row will sum to unity. If the elements $a_{i,i-1}$ and $a_{i,i+1}$ become larger than a_{min}, they are set to a_{min}, and the remaining $P-3$ elements are adjusted so that the rows sums to unity. This procedure continues until no elements of the row are larger than a_{min}.

Using the previously described elements, a_{ij}, the design parameters of $\mathbf{A}$ are the track termination and track initiation probabilities, u and v, and the degree of frequency changes as modeled by the standard deviation, d. Figure 1(a) shows an example of a state transition matrix.

Observation matrix

The $P \times P$ observation matrix $\mathbf{B}$ describes the probabilities of observing a specific state given the true state. Its elements, b_{ij}, corresponds to the probability of detection in state j when the true state is i. Furthermore, it is assumed that the signal is a sinusoid with added noise, defined by

$$s(n) = a\sin(2\pi f_0 n) + w(n). \tag{8}$$

The signal amplitude, a, and the frequency, f_0, are both assumed to be constant during the time period when one STFT slice is calculated. The noise, $w(n)$, is assumed to be zero-mean, Gaussian with variance σ^2. Hence, the discrete Fourier transform $S(f)$ of $s(n)$ is (see Appendix A)

$$\begin{aligned} S(f) &= \frac{1}{N}\sum_{n=0}^{N-1} s(n)e^{-j2\pi fn} \\ &= S_1(f) + S_1^*(-f) + \frac{1}{N}\sum_{n=0}^{N-1} w(n)e^{-j2\pi fn}, \end{aligned} \tag{9}$$

where

$$S_1(f) = \frac{a}{N2j}e^{j\pi(f_0-f)(N-1)} \cdot \frac{\sin(N\pi(f_0-f))}{\sin(\pi(f_0-f))}. \tag{10}$$

The Fourier transform $S(f)$ can be decomposed into signal and noise components, with magnitude and phase (C,ϕ) and (D,θ), respectively,

$$S(f) = C(f)e^{j\phi(f)} + D(f)e^{j\theta(f)} = R(f)e^{j\eta(f)}. \tag{11}$$

For $f_0 >> 0$, the magnitude of the signal component can be approximated by

$$C(f) \approx |S_1(f)| = \frac{a}{2N} \cdot \left| \frac{\sin(N\pi(f_0-f))}{\sin(\pi(f_0-f))} \right|, \quad f > 0. \tag{12}$$

Hence, the magnitude of the signal component of $S(f)$, can be simplified to

$$C(f) \approx \begin{cases} \frac{a}{2}, & \text{if signal present } (f = f_0); \\ 0, & \text{if signal absent } (f \neq f_0). \end{cases} \tag{13}$$

The distribution of the magnitude $R(f)$ is given by (see Appendix B)

$$p(R(f)) = \frac{2R(f)N}{\sigma^2} \cdot I_0\left(\frac{2R(f)C(f)N}{\sigma^2}\right) \cdot e^{-N\frac{R(f)^2+C(f)^2}{\sigma^2}}. \tag{14}$$

Using the approximated magnitudes of the signal component, the magnitude probability density function (PDF) becomes

$$p_1(R(f)) = \frac{2R(f)N}{\sigma^2} \cdot I_0\left(\frac{R(f)aN}{\sigma^2}\right) \cdot e^{-\frac{N(4R(f)^2+a^2)}{4\sigma^2}} \tag{15}$$

if the signal is present, i.e., $f = f_0$, and

$$p_2(R(f)) = \frac{2R(f)N}{\sigma^2} \cdot e^{-\frac{NR(f)^2}{\sigma^2}} \tag{16}$$

if the signal is absent, i.e., $f \neq f_0$.

The elements of $\mathbf{B}$ are derived from $p_1(R(f))$ and $p_2(R(f))$. If no signal is present, the probabilities of no detection (zero state), b_{00}, and detection in state i, b_{0i}, are given by

$$b_{00} = \prod_{i=1}^{P-1}\int_0^D p_2(r)dr = \left[1 - e^{-\frac{D^2 N}{\sigma^2}}\right]^{P-1}, \tag{17}$$

$$b_{0i} = \frac{1 - b_{00}}{P-1}, \tag{18}$$

respectively, where D denotes detection threshold.

If a signal with frequency between f_m and $f_m + \Delta f$ is present, the probabilities of detection in state m, b_{mm}, no detection (zero state), b_{m0}, and detection in state $i \neq m$, b_{mi}, are given by

$$b_{mm} = \int_D^\infty p_1(r)\prod_{i=1,i\neq m}^{P-1}\int_0^r p_2(r_1)dr_1 dr = \int_D^\infty p_1(r)\cdot\left[1 - e^{-\frac{r^2 N}{\sigma^2}}\right]^{P-2} dr, \tag{19}$$

$$b_{m0} = \int_0^D p_1(r)dr\prod_{i=1,i\neq m}^{P-1}\int_0^D p_2(r)dr = \left[1 - e^{-\frac{D^2 N}{\sigma^2}}\right]^{P-2}\int_0^D p_1(r)dr, \tag{20}$$

$$b_{m,i\neq m} = \frac{1 - b_{m0} - b_{mm}}{P-2}, \tag{21}$$

respectively.

The design parameters of $\mathbf{B}$ are the SNR, defined by a and σ^2, and D, see Fig. 1(b). As the SNR of the observation matrix increases, the observation matrix approaches the identity matrix, i.e., the observed states equal the true states.

Optimal detection threshold

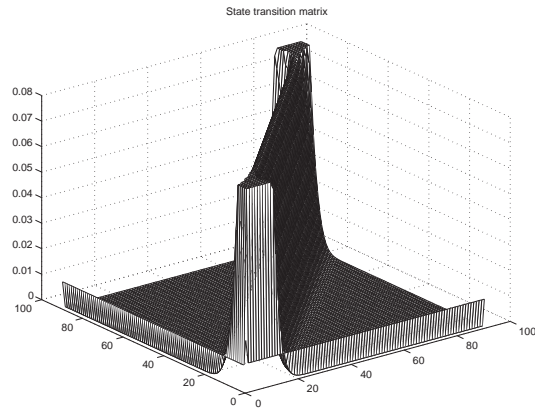An optimal detection threshold, D_{opt}, is determined for the following error cost function,

$$C_e = \alpha P_{FA} + \beta P_{FD}, \tag{22}$$

where the weights α and β sum to 1. The probabilities of false alarm and false detection can be expressed as
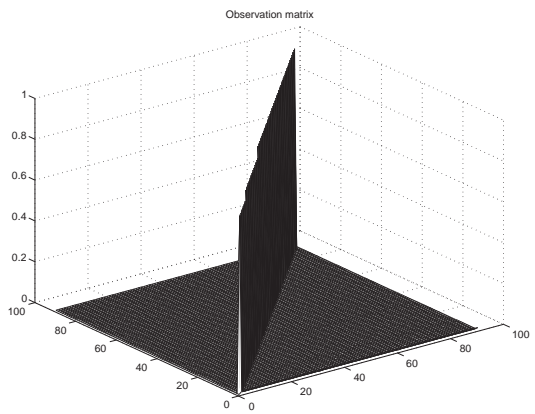
$$P_{FA} = p(R(f_1) > D \cap \cdots \cap R(f_{P-1}) > D | i = 0) = \mu_0\sum_{i=1}^{P-1} b_{0i} = \mu_0(1 - b_{00}), \tag{23}$$

and

$$P_{FD} = p(R(f_1) < D \cup \cdots \cup R(f_{P-1}) < D | i \neq 0) = \sum_{i=1}^{P-1}\mu_i b_{i0} = (1 - \mu_0)b_{i0}, \tag{24}$$

(a)

(b)

Figure 1: (a) The state transition matrix, $\mathbf{A}$, with $u = 0.98$, $v = 0.01$, and $d = 0.5$. (b) The observation matrix, $\mathbf{B}$, with $a = 0.1$, $\sigma^2 = 0.1$, and $D = 0.01$.

respectively, where $\boldsymbol{\mu} = [\mu_0, \mu_1, \ldots, \mu_n]^T$ is the long-term state probability vector. Hence, the error cost criterion can be expressed as

$$C_e \quad = \quad \alpha\mu_0(1 - b_{00}) + \beta(1 - \mu_0)b_{i0}. \tag{25}$$

The minimum can be found by setting the derivative of the cost function equal to zero,

$$\frac{\partial C_e}{\partial D} \quad = \quad -\alpha\mu_0\frac{\partial b_{00}}{\partial D} + \beta(1 - \mu_0)\frac{\partial b_{i0}}{\partial D} = 0, \tag{26}$$

where the derivatives are given by (see Appendix C)

$$\frac{\partial b_{00}}{\partial D} = \frac{2DN(P-1)}{\sigma^2}e^{-\frac{D^2N}{\sigma^2}}\left[1 - e^{-\frac{D^2N}{\sigma^2}}\right]^{-1}b_{00} \tag{27}$$

and

$$\frac{\partial b_{i0}}{\partial D} = \left[1 - e^{-\frac{D^2N}{\sigma^2}}\right]^{-1}\left(\frac{2DN(P-2)}{\sigma^2}e^{-\frac{D^2N}{\sigma^2}}b_{i0} + p_1(D)b_{00}\right), \tag{28}$$

respectively. Combining (26), (27), and (28) gives an expression of the probability of a magnitude equal to D when the signal is present,

$$p_1(D) = \frac{2DN(P-1)\alpha\mu_0}{\sigma^2\beta(1 - \mu_0)}e^{-\frac{D^2N}{\sigma^2}}\left(1 - \frac{\beta(1 - \mu_0)(P-2)b_{i0}}{\alpha\mu_0(P-1)b_{00}}\right). \tag{29}$$

The long-term probability of the zero state, μ_0 can be expressed as (see Appendix C)

$$\mu_0 = \frac{v}{u + v}, \tag{30}$$

where v and u are the track initiation and track termination probabilities. Hence,

$$p_1(D) = \frac{2DN(P-1)\alpha v}{\sigma^2\beta u}e^{-\frac{D^2N}{\sigma^2}}\left(1 - \frac{\beta u(P-2)b_{i0}}{\alpha v(P-1)b_{00}}\right). \tag{31}$$

By setting $\alpha = (1 - \mu_0)$ and $\beta = \mu_0$, false dismissals are emphasized if the probability of being in the zero state is small, and vice versa. Using these values of α and β,

$$p_1(D) \quad = \quad \frac{2DN(P-1)}{\sigma^2}e^{-\frac{D^2N}{\sigma^2}}\left(1 - \frac{(P-2)b_{i0}}{(P-1)b_{00}}\right). \tag{32}$$

The optimal threshold D_{opt} is then determined by

$$D_{opt} = \arg\max_D p_1(D). \tag{33}$$

Since b_{i0} and b_{00} depends on D, D_{opt} has to be calculated iteratively.

It can thus be shown that the cost function optimality criterion requires only the design parameters a and σ^2.

Initial state probability vector

To force automatic track initiation by starting in the zero state, the initial state probability vector, $\boldsymbol{\pi}$, is set to

$$\boldsymbol{\pi} = [a_{00}, a_{01}, \ldots, a_{0n}]^T = \left[1 - u, \frac{u}{P-1}, \ldots, \frac{u}{P-1}\right]^T. \tag{34}$$
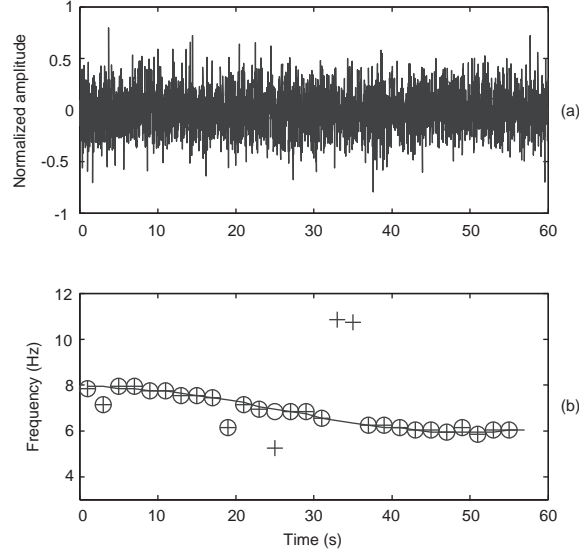
Figure 2: (a) A sinusoid signal ($a = 0.1$) embedded in white noise ($\sigma^2 = 0.2$). (b) The true frequency trend (solid line), the estimated frequency using STFT ('+'), and the estimated frequency using HMM ('o'). Note that absent '+' or 'o' corresponds to the zero state.

Viterbi track

Given an observed sequence, $\mathbf{z}$, an optimal sequence, $\mathbf{x}$, can be obtained using the Viterbi algorithm [15, 16]. This algorithm is initialized for $j = 0, 1, \ldots, P - 1$ with

$$\delta_1(j) = \ln \pi_j + \ln b_{j,z(1)}, \tag{35}$$
$$\psi_1(j) = 0, \tag{36}$$

where $\boldsymbol{\pi}$ is the initial state vector, $b_{j,z(1)}$ is element $(j, z(1))$ of $\mathbf{B}$, and $z(1)$ is the first element of $\mathbf{z}$. Then, for $t = 2, 3, \ldots, T$

$$\delta_t(j) = \ln b_{j,z(t)} + \max_{i=0,1,\ldots,P-1} \left(\delta_{t-1}(i) + \ln a_{ij} \right), \tag{37}$$
$$\psi_t(j) = \arg \max_{i=0,1,\ldots,P-1} \left(\delta_{t-1}(i) + \ln a_{ij} \right), \tag{38}$$

are defined for $j = 0, 1, \ldots, P - 1$, where $b_{j,z(t)}$ is element $(j, z(t))$ of $\mathbf{B}$, $z(t)$ is element number t of the observed sequence, and a_{ij} is element (i, j) of $\mathbf{A}$. The optimal sequence $\mathbf{x}$ is obtained using

$$x(T) = \arg \max_{j=0,1,\ldots,P-1} \left(\delta_T(j) \right), \tag{39}$$
$$x(t) = \psi_{t+1} \left(x(t+1) \right). \tag{40}$$

Figure 2 presents an example with a sinusoid, whose frequency is gradually decreasing, embedded in white noise. Three occurrences of extremely high and low spurious frequency estimates are avoided with the HMM. Figure 3 shows an example of a sinusoid with pronounced harmonics and gradually decreasing frequency embedded in white noise. At one occasion, the maximum peak
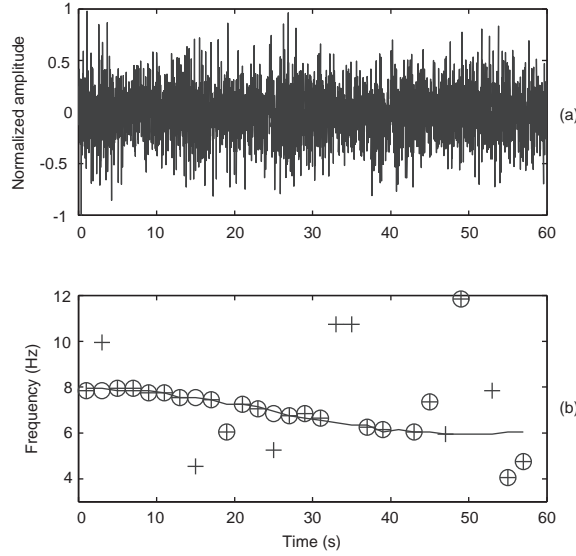
Figure 3: (a) A sinusoid signal with harmonics ($a_1 = 0.1, a_2 = 0.09, a_3 = 0.08$, defined in 41) embedded in white noise ($\sigma^2 = 0.2$). (b) The true frequency trend (solid line), the estimated frequency using STFT ('+'), and the estimated frequency using HMM ('o'). Note that absent '+' or 'o' corresponds to the zero state.

of the frequency spectrum is detected at the first harmonic and, incorrectly, verified by the HMM. Hence, erroneous detection of harmonic frequencies may be a problem in AF frequency tracking since the spectra often contain harmonics. The inclusion of harmonics in the HMM signal model may prevent such erroneous frequency estimates, see below.

2.2   An HMM for tracking a single frequency with harmonics

We assume that the signal consists of a sinusoid with $K - 1$ harmonics and noise, according to the following signal model

$$s(n) = \sum_{k=1}^{K} a_k \sin(2\pi k f_0 n) + w(n). \tag{41}$$

The amplitude of the signal, a_1, and its harmonics, $a_2, \ldots, a_K$, and the frequency f_0 is assumed to be constant during the time interval for the Fourier transform. The noise is assumed to be zero-mean, Gaussian with variance σ^2.

The discrete Fourier transform $S(f)$ of the signal $s(n)$ is

$$
\begin{aligned}
S(f) &= \frac{1}{N} \sum_{n=0}^{N-1} s(n) e^{-j2\pi fn} \\
&= \frac{1}{N} \sum_{n=0}^{N-1} \left(\sum_{k=1}^{K} a_k \sin(2\pi k f_0 n) + w(n) \right) e^{-j2\pi fn} \\
&= \sum_{k=1}^{K} \left(\frac{1}{N} \sum_{n=0}^{N-1} a_k \sin(2\pi k f_0 n) \right) + \frac{1}{N} \sum_{n=0}^{N-1} w(n) e^{-j2\pi fn} \\
&= \sum_{k=1}^{K} (S_k(f) + S_k^*(-f)) + \frac{1}{N} \sum_{n=0}^{N-1} w(n) e^{-j2\pi fn},
\end{aligned}
\tag{42}
$$

where

$$
S_k(f) = \frac{a_k}{2Nj} e^{j\pi(kf_0 - f)(N-1)} \frac{\sin(N\pi(kf_0 - f))}{\sin(\pi(kf_0 - f))}.
\tag{43}
$$

The magnitude of the signal component, $C(f)$, can then be approximated similar to the case without harmonics,

$$
C(f) \approx \begin{cases} \frac{a_k}{2}, & f = kf_0; \\ 0, & \text{otherwise.} \end{cases}
\tag{44}
$$

Hence, the magnitude PDF at $f = f_0$ or any of its harmonics, $p_{1k}, k = 1, \ldots, K$, is

$$
p_{1k}(R(f)) = \frac{2R(f)N}{\sigma^2} \cdot I_0 \left(\frac{R(f)a_k N}{\sigma^2} \right) \cdot e^{-\frac{N(4R(f)^2 + a_k^2)}{4\sigma^2}},
\tag{45}
$$

while the magnitude PDF at all other frequencies is identical to (16), i.e.,

$$
p_2(R(f)) = \frac{2R(f)N}{\sigma^2} \cdot e^{-\frac{NR(f)^2}{\sigma^2}}.
\tag{46}
$$

If no signal is present, the probability of no detection (zero state), b_{00}, and the probability of detection in state i, b_{0i} is identical to the case without harmonics, cf. (17) and (18), respectively. If a signal with frequency between f_m and $f_m + \Delta f$ is present, the probability of 1. detection in the frequency state or one of the harmonic states k, b_{mk}, where $f_k = k \cdot f_m, k = 1, \ldots, K$, 2. no detection (zero state), b_{m0}, and 3. detection in another state i, b_{mi}, where $f_i \neq k \cdot f_m$, are given by

$$
\begin{aligned}
b_{mk} &= \int_D^\infty p_{1k}(r) \prod_{i=1}^{P-K} \int_0^r p_2(r_1) dr_1 \prod_{j=1, j \neq k}^{K} \int_0^r p_{1h_j}(r_1) dr_1 dr \\
&= \int_D^\infty p_{1k}(r) \cdot \left[1 - e^{-\frac{r^2 N}{\sigma^2}} \right]^{P-K} \prod_{j=1, j \neq k}^{K} \int_0^r p_{1j}(r_1) dr_1 dr,
\end{aligned}
\tag{47}
$$

$$
\begin{aligned}
b_{m0} &= \prod_{i=1}^{P-K} \int_0^D p_2(r) dr \prod_{k=1}^{K} \int_0^D p_{1k}(r) dr \\
&= \left[1 - e^{-\frac{D^2 N}{\sigma^2}} \right]^{P-K} \prod_{k=1}^{K} \int_0^D p_{1k}(r) dr,
\end{aligned}
\tag{48}
$$

$$
b_{mi} = \frac{1 - b_{m0} - \sum_{k=1}^{K} b_{mk}}{P - 1 - K},
\tag{49}
$$
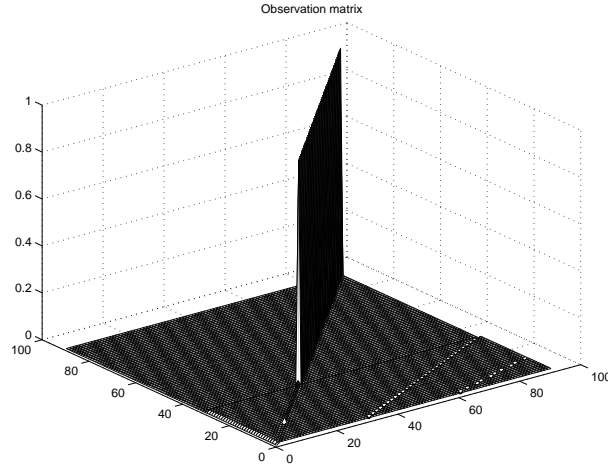
Figure 4: The observation matrix, $\mathbf{B}$, for the signal amplitude $a_1 = 0.1$, harmonic amplitudes, $a_2 = 0.09$ and $a_3 = 0.08$, the noise variance $\sigma^2 = 0.1$, and the detection threshold, $D = 0.01$.

respectively.

Figure 4 illustrates the observation matrix of a harmonic signal. Figure 5 shows an example of a sinusoid with strong harmonics and gradually decreasing frequency, embedded in white noise. In this example the false detection at the first harmonic is avoided. However, the effect of using an observation matrix designed to detect sinusoids with harmonics is relatively limited when compared to an observation matrix designed to detect a pure sinusoid. When the decay of the harmonics is larger, as is usually the case for AF signals, the effect becomes smaller.

2.3   Log-spectral template

The performance of HMM frequency tracking is compared to that of frequency tracking using the log-spectral template method [9], briefly summarized below. A spectrum, $\mathbf{q}_l$, is calculated for each segment of N samples of the residual ECG $\mathbf{x}_l$ using

$$\mathbf{q}_l = \mathbf{F}\mathbf{W}\mathbf{x}_l, \tag{50}$$

where the $K \times N$ matrix $\mathbf{F}$ defines the K-point discrete, nonuniform Fourier transform, and the elements of the $N \times N$ diagonal matrix $\mathbf{W}$ defines a window function. The transform matrix $\mathbf{F}$ is defined by
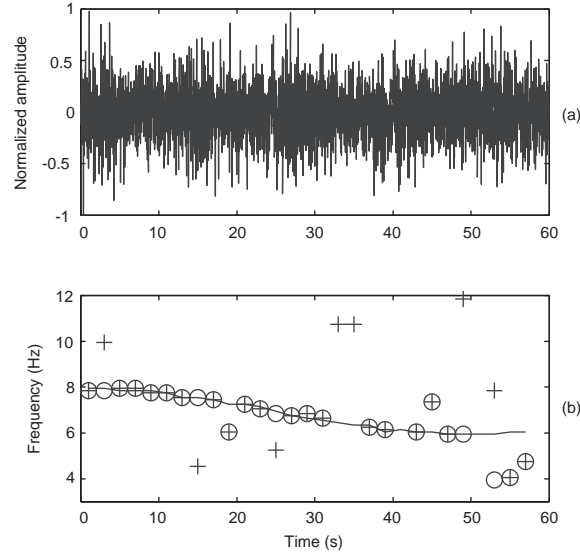
$$\mathbf{F} \;\; = \;\; \begin{bmatrix} \mathbf{1} & e^{-j2\pi\mathbf{f}} & e^{-j2\pi\mathbf{f}2} & \cdots & e^{-j2\pi\mathbf{f}(N-1)} \end{bmatrix}, \tag{51}$$

where $\mathbf{f} = [f_0, \ldots, f_{K-1}]^T$ is a logarithmically scaled frequency vector, with

$$f_k = f_0 \cdot 10^{\frac{k}{K}}, \quad k = 0, 1, \ldots, K - 1. \tag{52}$$

Each observed spectrum $\mathbf{q}_l$ can be modeled by $\tilde{\mathbf{q}}_l$ being a frequency-shifted, θ_l, and amplitude-scaled, a_l, version of a known real-valued spectral template, $\boldsymbol{\phi}_l$,

$$\tilde{\mathbf{q}}_l = a_l \, \mathbf{J}_{\theta_l} \, \boldsymbol{\phi}_l, \tag{53}$$

Figure 5: (a) A sinusoid signal with harmonics ($a_1 = 0.1, a_2 = 0.09, a_3 = 0.08$) embedded in white noise ($\sigma^2 = 0.2$). (b) The true frequency trend (solid line), the estimated frequency using STFT ('+'), and the estimated frequency using HMM designed for signals with harmonics ('o'). Note that absent '+' or 'o' corresponds to the zero state.

where the matrix $\mathbf{J}_{\theta_l}$ performs the frequency shift by selecting the appropriate interval of ϕ_l. The parameters a_l and θ_l are estimated so that $\tilde{\mathbf{q}}_l$ matches the true spectrum, $\mathbf{q}_l$ optimally in the least-squares sense.

For the first segment, the spectral template, ϕ_0, is initiated by setting it equal to a constant (=1) at the peak position and 0.01 at all other positions. The spectral template ϕ_l is then updated for each segment through exponential averaging. An estimate of the AF frequency is obtained by the peak position of the frequency-shifted spectral template.

3 Evaluation

3.1 Simulated signals

The frequency tracking methods are evaluated using simulated AF signals, to which either simulated or ECG-extracted noise is added. The AF signals are simulated as an amplitude varying sinusoid with M harmonics, where the fundamental AF frequency varies around F_0 with a maximum frequency deviation of ΔF and modulation frequency F_m [6]:

$$s(n) = -\sum_{k=1}^{M+1} a_k(n) \sin(2\pi \frac{F_0}{F_s} kn + \frac{\Delta F}{F_m} \sin(2\pi \frac{F_m}{F_s} n)). \tag{54}$$
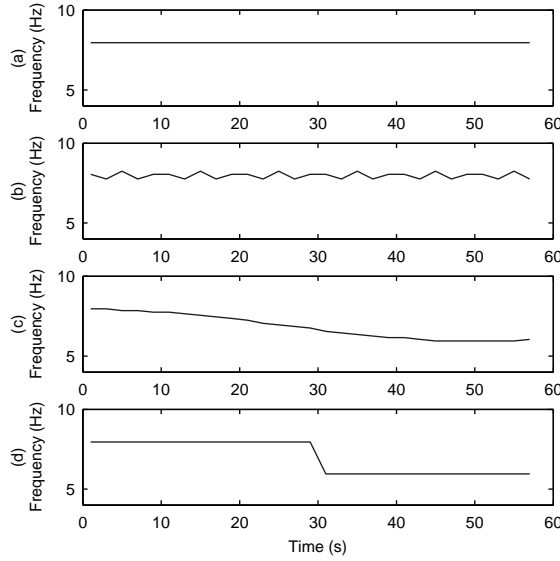
The time-varying amplitudes of the fundamental and the harmonics, denoted $a_1(n)$ and $a_k(n), k = 2, \ldots, M+1$, respectively, are given by

$$a_k(n) = e^{-\gamma k}(a + \Delta a \sin(2\pi \frac{F_a}{F_s} n)), \tag{55}$$

Table 1: Parameters of simulated AF signals. Note that the case "8/6 Hz" corresponds to 8 Hz at $0 < t < 30s$ and 6 Hz at $30 < t < 60s$.

Signal	f_0 (Hz)	Δf (Hz)	f_f (Hz)	a	Δa	f_a	γ
1	8	0	-	100	30	0.08	1
2	8	0.3	0.2	100	30	0.08	1
3	7	1	0.01	100	30	0.08	1
4	8/6	0	-	100	30	0.08	1

Figure 6: Frequency trends of the simulated AF signal with (a) constant frequency, (b) varying frequency, (c) gradually changing frequency, and (d) stepwise changing frequency.

where the amplitude Δa is the modulation peak amplitude and F_a is the modulation frequency. The exponential decay of the harmonic amplitudes is denoted γ.

Signals with four different frequency trends are created: constant frequency, varying frequency, gradually decreasing frequency, and stepwise decreasing frequency, see Tab. 1. The frequency trends of the simulated signals are displayed in Fig. 6.

The evaluation includes three different types of noise: white noise, remainders of QRST complexes, and muscular artifact noise, see Fig. 7. The QRST noise was obtained from ECG signals with normal sinus rhythm, where the QRST complexes were removed using average beat subtraction. The muscular artifact noise was obtained from the MIT-BIH stress test database [17]. For each type of noise, five different one-minute signals were used in the evaluation, normalized so that their variances were identical.

The SNR is defined by

$$SNR = 20 \log \frac{V_x}{\sigma_v}, \tag{56}$$

where V_x is the peak-to-peak amplitude of the simulated AF signal, and σ_v is the standard deviation
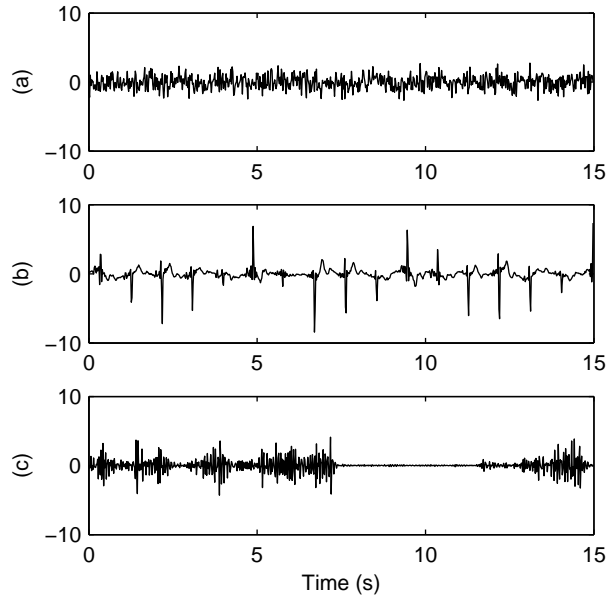
Figure 7: Noise excerpts defined by (a) white noise, (b) QRST remainders, and (c) muscular artifacts.

of the noise. Test signals were created with SNRs of 2–10 dB, except for white noise where the SNR started at 0 dB; these SNR values were considered as representative of observed signals. Figure 8 shows a simulated AF signal at an SNR of 5 dB.

4 Results

4.1 Parameter values

The frequency interval from 3 to 12 Hz is divided into segments of $\Delta f = 0.1$ Hz, so that state 1 corresponds to 3–3.1 Hz, and so on until state $P - 1$ which corresponds to 11.9–12 Hz. This gives a total of $P = 91$ states, including the zero state. The Fourier transform of the observed signal is calculated for every 2 second segment. The observed state is chosen in relation to the maximum peak of the periodogram if contained within 3–12 Hz and exceeding the detection threshold; otherwise the zero state is chosen.

Since AF is assumed to be present, the track initiation probability is set to $u = 0.98$ and the track termination probability to $v = 0.01$. Figure 9 shows an example of frequency tracking using different settings of the standard deviation d in **A**. With $d = 1$, only one erroneous frequency estimate is excluded, whereas several correct frequency estimates are slightly altered (i.e., on the order of 0.01 Hz) when $d = 0.1$. For $d = 0.1$, one erroneous frequency estimate is not excluded because it fits into an assumed change of the frequency trend. Hence, a large value of d implies that the HMM does not exclude or replace any frequency estimates, whereas actual changes in the frequency track are missed with too small a value of d. As a trade-off the standard deviation is set to $d = 0.5$ in this study.

An average RMS error is calculated for each type of noise, based on the mean RMS error of the four simulated frequency trends and the five different noise signals. The SNR of the observation matrix is a design parameter, defined by a and σ^2. Figure 10 shows the average RMS error of frequency
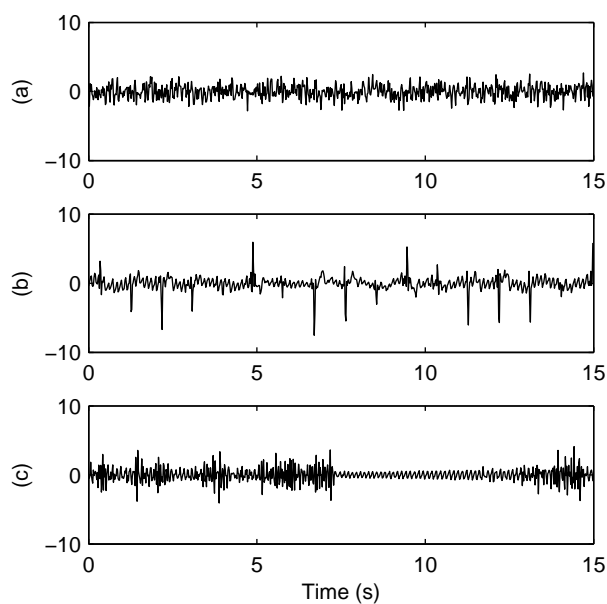
Figure 8: Simulated AF signals mixed with (a) white noise, (b) QRST remainders, and (c) muscular artifacts at an SNR of 5 dB.
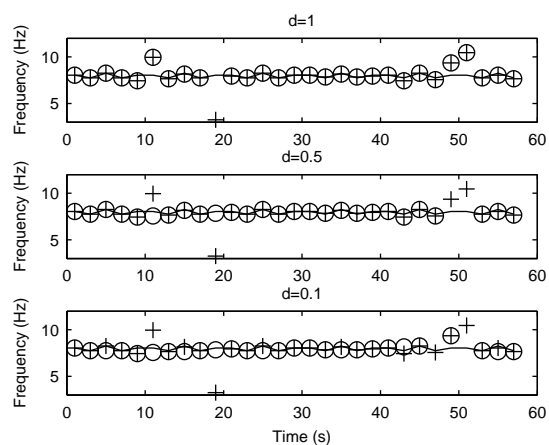
Figure 9: Frequency tracking illustrated for a simulated AF signal mixed with QRST remainder noise at an SNR of 5 dB, using different standard deviations, d, of the state transition matrix $\mathbf{A}$. The true frequency trend (solid line), the estimated frequency using STFT ('+'), and the estimated frequency using HMM designed for signals with harmonics ('o'). Note that absent '+' or 'o' corresponds to the zero state.
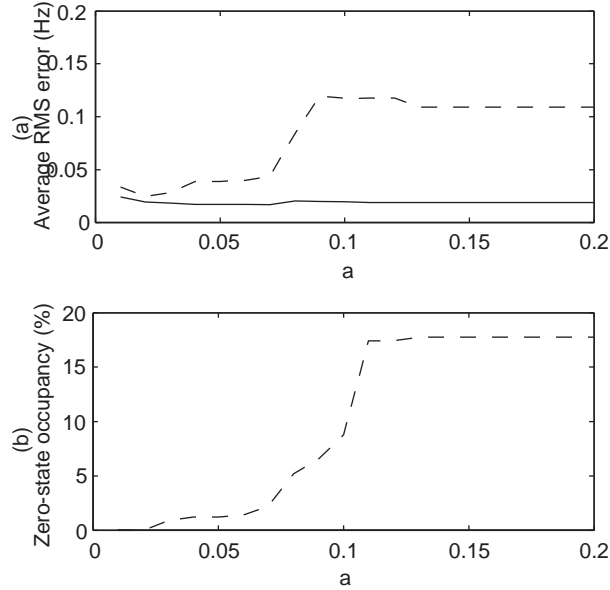
Figure 10: AF frequency tracking in QRST noise for different values of a ($\sigma^2 = 0.1$).
(a) The average RMS error at an SNR of 4 dB (solid line) and 2 dB (dashed line), and
(b) the corresponding zero state occupancy.

tracking of AF mixed with QRST noise to an SNR of 2 and 4 dB, respectively, using a fixed value of $\sigma^2 (= 0.1)$ and different values of a. It is evident that the best average performance is achieved when a is low, i.e., smaller than 0.1. However, choosing too low a value of a prevents tracking of fast changes in the frequency trend. Figure 11 illustrates the trade-off between robustness to noise and ability to track fast changes associated with different values of a. Since tracking performance is similar for $a > 0.1$, the signal and noise amplitudes of $\mathbf{B}$ are set to $a_1 = 0.1$, $a_2 = 0.04$, $a_3 = 0.01$ and $\sigma^2 = 0.1$, respectively. This yields an SNR of approximately -10 dB. The decrease in amplitude of the harmonics corresponds to an approximate exponential decay of $\gamma = 1$.

4.2 SNR

HMM-based frequency tracking is exemplified for different SNRs in Fig. 12, using QRST remainder noise. At 10 dB SNR, no erroneous frequency estimates occur, and consequently the HMM has no effect. At 5 dB SNR, two erroneous frequency estimate are replaced by estimates determined by the HMM, and two erroneous frequency estimates are excluded by the HMM, i.e., set to the zero state. At 0 dB SNR, several erroneous frequency estimates are either excluded or replaced by frequencies better fitting the trend.

The average RMS error of the estimated frequencies of simulated AF signals mixed with white noise is presented in Fig. 13 for the HMM method. A high zero state occupancy percentage tends to give a lower average RMS error, since the error is undefined at zero state. Therefore, it is important to compare not only the average RMS error, but also the zero state occupancy percentage. An observation matrix with $a = 0.05$ yields a lower average RMS error, and a lower zero state occupancy than does $a = 0.1$, whereas $a = 0.05$ reduces the ability to track fast changes in frequency, see Fig. 11.

The average RMS error of the estimated frequencies of simulated AF signals mixed with noise
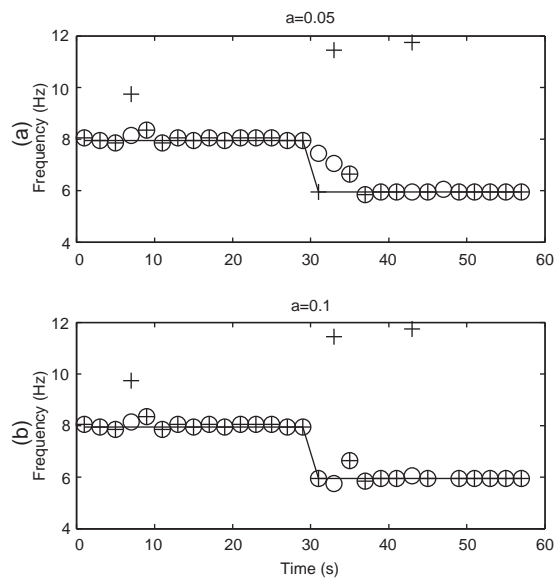
Figure 11: Tracking of a frequency step change in white noise at an SNR of 5 dB, for two different values of a ($\sigma^2 = 0.1$). The true frequency trend (solid line), the estimated frequency using STFT ('+'), and estimated frequency using HMM ('o') with (a) $a = 0.05$ and (b) $a = 0.1$.
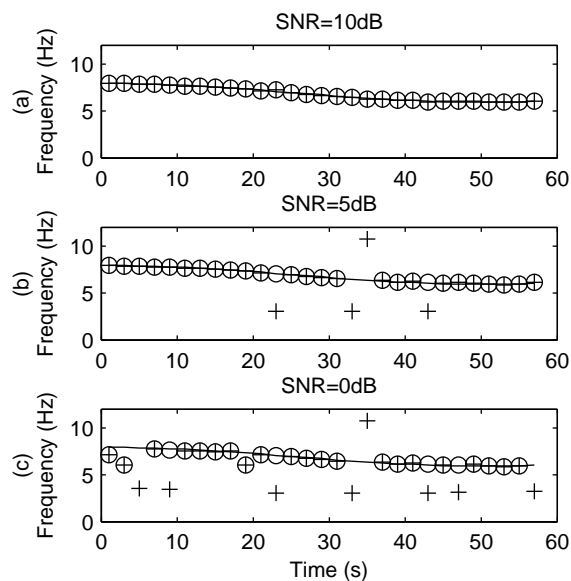
Figure 12: Frequency tracking with and without employing the HMM of simulated AF signals mixed with QRST-noise to (a) 10 dB SNR, (b) 5 dB SNR and (c) 0 dB SNR. The true frequency trend (solid line), the estimated frequency using STFT ('+'), and the estimated frequency using HMM ('o'). Note that absent '+' or 'o' corresponds to zero state.
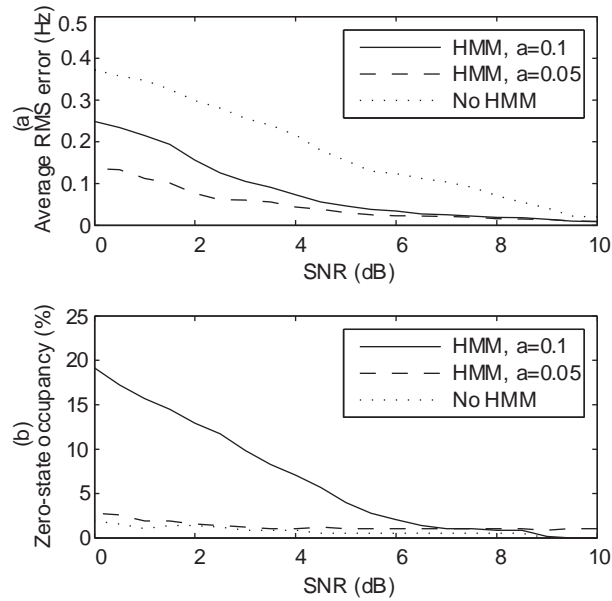
Figure 13: (a) RMS error and (b) zero state occupancy as function of SNR for simulated AF with white noise. The zero state occupancy at input is denoted 'no HMM'.

due to muscular artifacts is presented in Fig. 14 for the HMM, the spectral template method, and the STFT. It is evident that the HMM frequency tracker performs better than both the STFT and the spectral template method in muscular artifact noise.

For simulated AF signals mixed with QRST remainder noise, the resulting average RMS error is presented in Fig. 15, yielding a result similar to that in Fig. 14. However, it should be noted that the average RMS error of the spectral template frequency estimates is considerably lower for QRST noise than for muscular artifact noise.

In general, the RMS error does not differ much between the four different types of frequency trends. However, the combination of a varying AF frequency (Fig. 6(b)) with QRST remainder noise leads to an RMS error that increases faster at very low SNRs than for the other types of frequency trends, see Fig. 16.

5 Discussion

HMMs were originally suggested for use in the field of speech signal processing, but have since been applied to various biomedical signal processing problems, e.g., ECG segmentation [18, 19], cardiac arrhythmia analysis [20], EEG classification [21], and recognition of sleep stages [22]. The application of HMMs in AF analysis is, to our knowledge, novel to this paper.

The AF frequency plays a central role when analyzing AF from the ECG. In a previous study, we found that a lower AF frequency indicates a higher likelihood of spontaneous termination [5]. Other studies have shown a correlation between AF frequency and likelihood of drug-induced termination [3,4]. Therefore, it is important to reliably estimate the AF frequency. It is also of great interest to study how the AF frequency changes over longer time periods. However, a common problem in ambulatory recordings is noise which corrupts the AF frequency estimates.

This work extends the HMM proposed by Streit et. al. for frequency tracking of a sinusoid in white noise [10] to tracking of a sinusoid with harmonics. The effect of using an observation
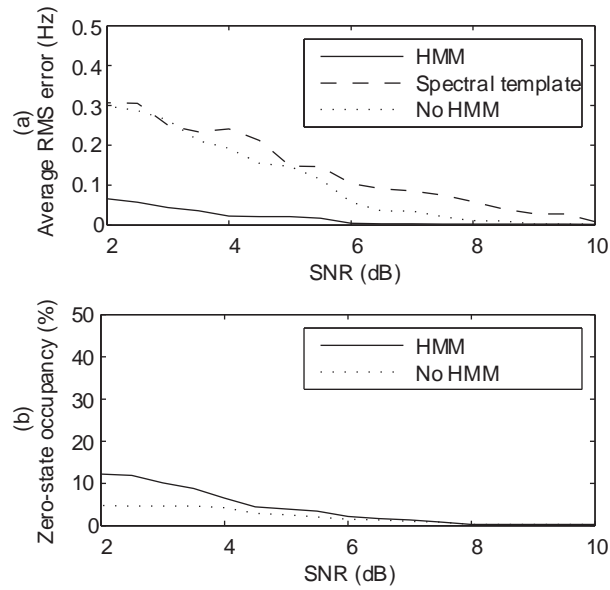
Figure 14: (a) RMS error and (b) zero state occupancy as function of SNR for simulated AF with muscular artifacts.
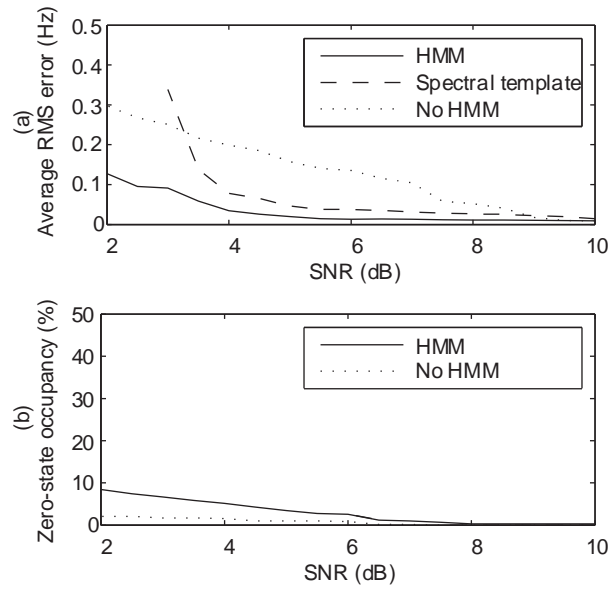
Figure 15: (a) RMS error and (b) zero state occupancy as function of SNR for simulated AF with QRST remainders.
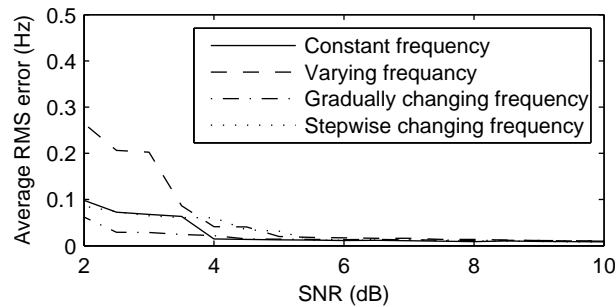
Figure 16: RMS error as function of SNR for the four different simulated AF frequency trends with QRST remainders.

matrix designed to detect sinusoids with harmonics, compared to an observation matrix designed to detect sinusoids, turned out to be limited. When the decay of the harmonics is large, as is often the case for AF signals, the improvement is marginal. However, it is more suitable to use an HMM designed to detect sinusoids with harmonics for an atrial flutter signal, whose harmonics are much more pronounced. Frequency tracking of intra-atrial fibrillation signals, for which the amplitude of the harmonics may be larger than the fundamental, is another potential application of our extended HMM [23].

Even though our model is designed for white noise, it performs well for other types of noise. Noise due to QRST remainders and muscular artifacts typically consist of infrequent high level intermittent spike artifacts. In between these spikes, the noise level is low and the fibrillation signal is clearly visible. Since the SNR definition is based on the average power of the noise, signal detection is generally easier for non-Gaussian noise than for Gaussian noise at the same SNR [24].

The tracking performance of the HMM is sensitive to the choice of a, σ^2, and d. The values of a and σ^2 correspond to a lower SNR than the actual SNR of the simulated signals. The best tracking performance is not necessarily attained when a and σ^2 corresponds to the SNR of the simulated signal, cf. Fig. 10.

The HMM is tested on simulated AF signals with step-wise changing frequency, showing that the HMM is able to track sudden changes of the AF frequency trend. However, choosing too low a value of the design parameter a of the observation matrix precludes detection of fast changes in the frequency trend, see Fig. 11.

The HMM can be designed so that short-time frequency estimates which do not fit the frequency trend are excluded or replaced by frequencies which better fit the trend. This can be done by adjusting the parameter d in the state transition matrix, describing the likelihood of AF frequency change. The frequency tracking performance is sensitive to the choice of d, see Fig. 9.

For all tested cases, frequency tracking with HMM is associated with significantly lower RMS errors at low SNRs than is tracking without. The difference in performance is negligible when tracking the different types of frequency trends, except for the case with varying AF frequency mixed with QRST remainder noise. In this particular case, the faster performance deterioration at low SNRs is explained by the fact that this type of frequency trend produces the most nonstationary signal.

The HMM method and the spectral template method exhibit similar performance when processing signals with QRST remainder noise for most SNRs of practical significance (Fig. 15(a)). This result is to be expected when considering that the spectral template method was designed to deal with such noise in particular. However, the performance difference becomes quite substantial at very low SNRs, i.e., below 4 dB, or in the presence muscular artifacts (Fig. 14(a)).

The present performance evaluation involves simulated AF signals, i.e., defined by a sum of

weighted sinusoids, to which different types of real-life noise have been added. Evidently, such an evaluation offers the important advantage of describing the performance in quantitative results, using e.g., the error between the underlying AF frequency and the estimated. Since the atrial fibrillatory activity is much more complex in reality than what can be accounted for by the sinusoidal model, a complete performance evaluation of HMM-based frequency tracking should, in the future, also involve the analysis of ECG signals. However, such an evaluation also has to address the problem of expressing the performance in quantitative terms.

Other methods for reducing false short-time AF frequency estimates may be to lowpass filter the frequency trend, or to simply remove outlier values, i.e., short-time frequency estimates that differ significantly from the frequency trend. However, it is difficult to set general values of thresholds and filter parameters, since changes of the frequency trend due to, e.g., drug administration, must be allowed. Also, there are large variations between different patients.

6   Conclusions

Using an HMM for frequency tracking of AF in the ECG significantly lowers the RMS error. Hence, this approach may have important implications for future analysis of ambulatory ECGs with AF. With an adequate choice of design parameter values, the HMM is able to track sudden changes of the fibrillation frequency. Although inclusion of harmonics in the model did not improve the tracking performance appreciably, it performed equally well as the HMM designed for frequency tracking of a signal without harmonics.

A   Observation matrix

The discrete Fourier transform $S(f)$ of the signal $s(n)$ is

$$
\begin{aligned}
S(f) &= \frac{1}{N} \sum_{n=0}^{N-1} s(n) e^{-j2\pi f n} \\
&= \frac{1}{N} \sum_{n=0}^{N-1} \left(a \sin(2\pi f_0 n) + w(n) \right) e^{-j2\pi f n}.
\end{aligned}
\tag{57}
$$

The Euler formula gives that the first term equals

$$
\begin{aligned}
&\frac{1}{N} \sum_{n=0}^{N-1} a \sin(2\pi f_0 n) e^{-j2\pi f n} \\
&= \frac{1}{N} \sum_{n=0}^{N-1} \frac{a}{2j} \left(e^{j2\pi f_0 n} - e^{-j2\pi f_0 n} \right) e^{-j2\pi f n} \\
&= \frac{a}{N2j} \sum_{n=0}^{N-1} e^{j2\pi(f_0 - f)n} - \frac{a}{N2j} \sum_{n=0}^{N-1} e^{-j2\pi(f_0 + f)n}.
\end{aligned}
\tag{58}
$$

Summation of the geometric terms gives that

$$
\begin{aligned}
&\frac{a}{N2j}\frac{1-e^{j2\pi(f_0-f)N}}{1-e^{j2\pi(f_0-f)}} - \frac{a}{N2j}\frac{1-e^{-j2\pi(f_0+f)N}}{1-e^{-j2\pi(f_0+f)}} \\
=\ &\frac{a}{N2j}\frac{e^{j\pi(f_0-f)N}}{e^{j\pi(f_0-f)}}\cdot\frac{e^{-j\pi(f_0-f)N}-e^{j\pi(f_0-f)N}}{e^{-j\pi(f_0-f)}-e^{j\pi(f_0-f)}} - \\
&\frac{a}{N2j}\frac{e^{-j\pi(f_0+f)N}}{e^{-j\pi(f_0+f)}}\cdot\frac{e^{j\pi(f_0+f)N}-e^{-j\pi(f_0+f)N}}{e^{j\pi(f_0+f)}-e^{-j\pi(f_0+f)}} \\
=\ &\frac{a}{N2j}e^{j\pi(f_0-f)(N-1)}\cdot\frac{\sin(N\pi(f_0-f))}{\sin(\pi(f_0-f))} + \\
&\frac{a}{N2j}e^{-j\pi(f_0+f)(N-1)}\cdot\frac{\sin(N\pi(f_0+f))}{\sin(\pi(f_0+f))}.
\end{aligned}
\tag{59}
$$

Hence, the discrete Fourier transform is

$$
S(f) \;=\; S_1(f) + S_1^*(-f) + \frac{1}{N}\sum_{n=0}^{N-1}w(n)e^{-j2\pi fn},
\tag{60}
$$

where

$$
S_1(f) = \frac{a}{N2j}e^{j\pi(f_0-f)(N-1)}\cdot\frac{\sin(N\pi(f_0-f))}{\sin(\pi(f_0-f))}.
\tag{61}
$$

B   Joint magnitude

We want to find the PDF, $p(z)$, of the radius $z = \sqrt{x^2+y^2}$, where x and y are independent with Gaussian distribution and equal variance σ^2. The mean-values are $E[x] = \eta$, $E[y] = 0$ respectively. Then, x and y have the joint PDF

$$
p(x,y) = \frac{1}{2\pi\sigma^2}e^{-\frac{(x-\eta)^2+y^2}{2\sigma^2}}.
\tag{62}
$$

To find $p(z)$ we integrate $p(x,y)$ over ΔD_z, where

$$
\Delta D_z : z < \sqrt{x^2+y^2} \le z+dz, \quad z > 0.
\tag{63}
$$

Hence

$$
\begin{aligned}
p(z)dz &= \int\!\!\int_{\Delta D_z} p(x,y)dxdy \\
&= \frac{1}{2\pi\sigma^2}\int_0^{2\pi} e^{-\frac{(z\cos\theta-\eta)^2+(z\sin\theta)^2}{2\sigma^2}} z\,dz\,d\theta,
\end{aligned}
\tag{64}
$$

where the last step uses the following change of variables

$$
\begin{aligned}
x &= z\cos\theta, & \tag{65}\\
y &= z\sin\theta, & \tag{66}\\
dxdy &= z\,dz\,d\theta. & \tag{67}
\end{aligned}
$$

This results in

$$
\begin{aligned}
p(z) &= \frac{1}{2\pi\sigma^2} \int_0^{2\pi} e^{\frac{-(z\cos\theta - \eta)^2 + (z\sin\theta)^2}{2\sigma^2}} z\,d\theta \\
&= \frac{z}{2\pi\sigma^2} e^{-\frac{z^2+\eta^2}{2\sigma^2}} \int_0^{2\pi} e^{\frac{z\eta\cos\theta}{\sigma^2}} \\
&= \frac{z}{\sigma^2} e^{-\frac{z^2+\eta^2}{2\sigma^2}} \cdot I_0\left(\frac{z\eta}{\sigma^2}\right), \quad z > 0,
\end{aligned}
\tag{68}
$$

where I_0 is the modified Bessel function of order 0,

$$
I_0(x) = \frac{1}{2\pi} \int_0^{2\pi} e^{x\cos\theta} d\theta = \sum_{n=0}^{\infty} \frac{x^{2n}}{2^{2n}(n!)^2}.
\tag{69}
$$

In this case, x is the signal with half of the noise, $E[x] = C$ and y is the other half of the noise, $E[y] = 0$. The variance of the two variables is $\sigma^2/2N$ and the radius $z = R$. This gives an expression of the PDF of the magnitude R, $p(R)$,

$$
\begin{aligned}
p(R) &= \frac{R}{\sigma^2/2N} \cdot I_0\left(\frac{RC}{\sigma^2/2N}\right) \cdot e^{-\frac{R^2+C^2}{2\sigma^2/2N}} \\
&= \frac{2RN}{\sigma^2} \cdot I_0\left(\frac{2RCN}{\sigma^2}\right) \cdot e^{-N\frac{R^2+C^2}{\sigma^2}}.
\end{aligned}
\tag{70}
$$

C   Optimal detection threshold

C.1   Long-term state probability

The long-term state probability vector, $\boldsymbol{\mu}$, sums up to unity and satisfies the equation

$$
\boldsymbol{\mu} = \boldsymbol{\mu}\mathbf{A}.
\tag{71}
$$

Hence, the long-term probability of the zero state, i.e., no signal present, μ_0, must satisfy

$$
\begin{aligned}
\mu_0 &= \sum_{i=0}^{n} \mu_i a_{i0} \\
&= (1-u)\mu_0 + v\sum_{i=1}^{n} \mu_i \\
&= (1-u)\mu_0 + v(1-\mu_0).
\end{aligned}
\tag{72}
$$

This results in that

$$
\mu_0 = \frac{v}{u+v}.
\tag{73}
$$

C.2   Derivatives of $b00$ and $bi0$

The error cost criterion,

$$
C_e = \alpha\mu_0(1 - b_{00}) + \beta(1 - \mu_0)b_{i0},
\tag{74}
$$

is minimized with respect to D, setting the derivative to zero,

$$
\frac{\partial C_e}{\partial D} = -\alpha\mu_0 \frac{\partial b_{00}}{\partial D} + \beta(1 - \mu_0)\frac{\partial b_{i0}}{\partial D} = 0,
\tag{75}
$$

where

$$\begin{aligned}
\frac{\partial b_{00}}{\partial D} &= \frac{\partial}{\partial D}\left(\left[1-e^{-\frac{D^2 N}{\sigma^2}}\right]^{P-1}\right) \\
&= (P-1)\left[1-e^{-\frac{D^2 N}{\sigma^2}}\right]^{P-2}\frac{2DN}{\sigma^2}e^{-\frac{D^2 N}{\sigma^2}} \\
&= \frac{2DN(P-1)}{\sigma^2}e^{-\frac{D^2 N}{\sigma^2}}\left[1-e^{-\frac{D^2 N}{\sigma^2}}\right]^{-1}b_{00},
\end{aligned} \tag{76}$$

and

$$\begin{aligned}
\frac{\partial b_{i0}}{\partial D} &= \frac{\partial}{\partial D}\left(\left[1-e^{-\frac{D^2 N}{\sigma^2}}\right]^{P-2}\int_0^D p_1(r)dr\right) \\
&= (P-2)\left[1-e^{-\frac{D^2 N}{\sigma^2}}\right]^{P-3}\frac{2DN}{\sigma^2}e^{-\frac{D^2 N}{\sigma^2}}\int_0^D p_1(r)dr + \left[1-e^{-\frac{D^2 N}{\sigma^2}}\right]^{P-2}p_1(D) \\
&= \left[1-e^{-\frac{D^2 N}{\sigma^2}}\right]^{-1}\left(\frac{2DN(P-2)}{\sigma^2}e^{-\frac{D^2 N}{\sigma^2}}b_{i0}+p_1(D)b_{00}\right).
\end{aligned} \tag{77}$$

Hence,

$$\begin{aligned}
\frac{\partial C_e}{\partial D} &= -\alpha\mu_0\frac{2DN(P-1)}{\sigma^2}e^{-\frac{D^2 N}{\sigma^2}}\left[1-e^{-\frac{D^2 N}{\sigma^2}}\right]^{-1}b_{00} \\
&\quad +\beta(1-\mu_0)\left[1-e^{-\frac{D^2 N}{\sigma^2}}\right]^{-1}\left(\frac{2DN(P-2)}{\sigma^2}e^{-\frac{D^2 N}{\sigma^2}}b_{i0}+p_1(D)b_{00}\right).
\end{aligned} \tag{78}$$

Setting equal to zero to find minimum of C_e gives

$$\begin{aligned}
p_1(D) &= \frac{1}{\beta(1-\mu_0)b_{00}}\left(\alpha\mu_0\frac{2DN(P-1)}{\sigma^2}e^{-\frac{D^2 N}{\sigma^2}}b_{00}-\beta(1-\mu_0)\frac{2DN(P-2)}{\sigma^2}e^{-\frac{D^2 N}{\sigma^2}}b_{i0}\right) \\
&= \frac{2DN(P-1)\alpha\mu_0}{\sigma^2\beta(1-\mu_0)}e^{-\frac{D^2 N}{\sigma^2}}\left(1-\frac{\beta(1-\mu_0)(P-2)b_{i0}}{\alpha\mu_0(P-1)b_{00}}\right) \\
&= \frac{2DN(P-1)\alpha v}{\sigma^2\beta u}e^{-\frac{D^2 N}{\sigma^2}}\left(1-\frac{\beta u(P-2)b_{i0}}{\alpha v(P-1)b_{00}}\right).
\end{aligned} \tag{79}$$

References

[1] V. Fuster *et al.*, "ACC/AHA/ESC guidelines for the management of patients with atrial fibrillation," *Circ.*, vol. 104, pp. 2118–2150, 2001.

[2] J. Slocum, E. Byrom, L. McCarthy, A. Sahakian, and S. Swiryn, "Computer detection of atrioventricular dissociation from surface electrocardiograms during wide QRS complex tachycardia," *Circ.*, vol. 72, pp. 1028–1036, 1985.

[3] A. Bollmann, N. Kanuru, K. McTeague, P. Walter, D. B. DeLurgio, and J. Langberg, "Frequency analysis of human atrial fibrillation using the surface electrocardiogram and its response to ibutilide," *Am. J. Cardiol.*, vol. 81, pp. 1439–1445, 1998.

[4] A. Bollmann, K. Binias, I. Toepffer, J. Molling, C. Geller, and H. Klein, "Importance of left atrial diameter and atrial fibrillatory frequency for conversion of persistent atrial fibrillation with oral flecainide," *Am. J. Cardiol.*, vol. 90, pp. 1011–1014, 2002.

[5] F. Nilsson, M. Stridh, A. Bollmann, and L. Sörnmo, "Predicting spontaneous termination of atrial fibrillation using the surface ECG," *Med. Eng. Physics*, vol. 28, pp. 802–808, 2006.

[6] M. Stridh and L. Sörnmo, "Spatiotemporal QRST cancellation techniques for analysis of atrial fibrillation," *IEEE Trans. Biomed. Eng.*, vol. 48, pp. 105–111, 2001.

[7] P. Langley, J. P. Bourke, and A. Murray, "Frequency analysis of atrial fibrillation," in *Proc. Computers in Cardiology*. IEEE Press, 2000, pp. 65–68.

[8] J. J. Rieta, V. Zarzoso, J. Millet-Roig, R. Garcia-Civera, and R. Ruiz-Granell, "Atrial activity extraction based on blind source separation as an alternative QRST cancellation for atrial fibrillation analysis," in *Proc. Computers in Cardiology*. IEEE Press, 2000, pp. 69–72.

[9] M. Stridh, L. Sörnmo, C. J. Meurling, and S. B. Olsson, "Sequential characterization of atrial tachyarrhythmias based on ECG time-frequency analysis," *IEEE Trans. Biomed. Eng.*, vol. 51, pp. 100–114, 2004.

[10] R. L. Streit and R. F. Barrett, "Frequency line tracking using hidden Markov models," *IEEE Trans. Acoust., Speech, Signal Processing*, vol. 38, pp. 586–598, 1990.

[11] X. Xie and R. J. Evans, "Multiple target tracking and multiple frequency line tracking using Hidden Markov Models," *IEEE Trans. Sig. Proc.*, vol. 39, pp. 2659–2676, 1991.

[12] ——, "Multiple frequency line tracking with hidden Markov models - further results," *IEEE Trans. Sig. Proc.*, vol. 41, pp. 334–343, 1993.

[13] R. F. Barrett and D. A. Holdsworth, "Frequency tracking using hidden Markov models with amplitude and phase information," *IEEE Trans. Sig. Proc.*, vol. 41, pp. 2965–2976, 1993.

[14] S. Paris and C. Jauffret, "Frequency line tracking using HMM-based schemes," *IEEE Trans. Aerosp. Electron. Syst.*, vol. 39, pp. 439–449, 2003.

[15] L. Rabiner and B. H. Juang, "An introduction to hidden Markov models," *IEEE ASSP Magazine*, pp. 4–19, 1986.

[16] G. D. Forney, "The Viterbi algorithm," *IEEE Proc.*, vol. 61, pp. 268–278, 1973.

[17] A. L. Goldberger, L. A. N. Amaral, L. Glass, J. M. Hausdorff, P. C. Ivanov, R. G. Mark, J. E. Mietus, G. B. Moody, C.-K. Peng, and H. E. Stanley, "PhysioBank, PhysioToolkit, and PhysioNet: Components of a new research resource for complex physiologic signals," *Circ.*, vol. 101, pp. e215–e220, 2000.

[18] S. Graja and J.-M. Boucher, "Multiscale hidden Markov model applied to ECG segmentation," in *Proc. WISP*, 2003, pp. 105–109.

[19] A. Koski, "Modelling ECG signals with hidden Markov models," *Aritficial Intelligence in Medicine*, vol. 8, pp. 453–471, 1996.

[20] D. Coast, R. Stern, G. Cano, and S. Briller, "An approach to cardiac arrhythmia analysis using hidden Markov models," *IEEE Trans. Biomed. Eng.*, vol. 37, pp. 826–836, 1990.

[21] B. Obermaier, C. Guger, C. Neuper, and G. Pfurtscheller, "Hidden Markov models for online classification of single trial EEG data," *Pattern Recogn. lett.*, vol. 22, pp. 1299–1309, 2001.

[22] A. Cohen, "Hidden Markov models in biomedical signal processing," in *Proc. EMBS*. IEEE Eng. Med. Biol. Soc., 1998, pp. 1145–1150.

[23] M. Stridh, A. Bollmann, D. Husser, A. Bhandari, D. Cannom, and L. Sörnmo, "Time-frequency characterization of simultaneous intra-atrial and electrocardiographic recordings during atrial fibrillation," in *Proc. Computers in Cardiology*. IEEE Press, 2005, pp. 347–350.

[24] S. Kay, *Fundamentals of statistical signal processing - Detection theory*. Prentice Hall, 1993, vol. 2.